Electronic Supporting Information

Why Triage the Materials with Low Luminescence Quantum Efficiency: The Use of 35Cbz4BzCN as a Universal Host for Organic Light Emitting Diode through Effective Triplet Energy Transfer

Yi-Mei Huang[a], Tse-Ying Chen[d], Deng-Gao Chen[a], Hsuan-Chi Liang[a], Cheng-Ham Wu[a], Mandy M. Lee [e], Tien-Lung Chiu*[,c], Jiun-Haw Lee*[,b], Yu-Cheng Chiu*[,d], Pi-Tai Chou*[,a] and Man-kit Leung*[,]

a. Department of Chemistry and b. Graduate Institute of Photonics and Optoelectronics, Department of Electrical Engineering, National Taiwan University, Taipei 10617, Taiwan. c. Department of Electrical Engineering, Yuan Ze University, Taoyuan 32003, Taiwan. d. Department of Chemical Engineerin, National Taiwan University of Science and Technology, Taipei 10607, Taiwan. e. Institute of Chemistry, Academia Sinica, Academia Sinica, Taipei 115, Taiwan.

Table of Contents

Synthesis

3,5-difluoro-4-(1-phenyl-1H-benzo[d]imidazol-2-yl)benzonitrile)(35F4BzCN)

3,5-Difluoro-4-formylbenzonitrile (1.67 g, 10 mmol, 1 equiv) and 2-aminodiphenlamine (2.02 g, 11 mmol, 1.1 equiv) were reacted in a solution of DMF (45 mL) and H_2O (5 mL) at 80 ^oC under an air atmosphere for 2.5 hours. The solvent was removed by vacuum distillation. The residue was dissolved in dichloromethane and washed with water twice. The organic layer was then dried over anhydrous $MgSO_4$ and concentrated by rotary evaporation. The crude product was purified by chromatography on silica gel, using hexanes/ethylacetate = 3/1 to 2/1 as eluent to afford essentially pure **35F4BzCN** (0.9 g, 54 %) as a white powder: m.p. 206.0 - 206.5 ℃; ^1H NMR (400 MHz, Acetone-d6): δ 7.88-7.85 (m, 1 H), 7.71-7.67 (m, 2 H), 7.58-7.49 (m, 3 H), 7.42-7.40 (m, 5 H); ^{13}C NMR (100 MHz, Acetone-d6): δ 162.95 (d, JCF = 7 Hz) , 160.4 (d, JCF = 7 Hz), 144.48, 144.41, 137.12, 136.30, 130.70, 130.04, 130.04, 127.28, 125.33, 124.129, 121.25, 117.38, 117.10, 116.89, 111.68; HRMS calcd for $C_{20}H_{11}F_2N_3$ ($M+1^+$) 332.0999, obsd 332.0998.

3,5-di(9H-carbazol-9-yl)-4-(1-phenyl-1H-benzo[d]imidazol-2-yl)benzonitrile(35Cbz4BzCN)

To a mixture of carbazole (0.70 g, 4.2 mmol, 1 equiv) and Cs_2CO_3 (1.42 g, 4.2 mmol, 2.1 equiv) in DMF (6 mL) was added a solution of **35F4BzCN** (0.66 g, 2 mmol, 1 equiv) in DMF (4 mL). The mixture was stirred at 80℃ under argon for 8 hours. Removal of the solvent by vacuum distillation had given a residue that was re-dissolved in DCM and washed with water. The organic layer was then dried over anhydrous $MgSO_4$.and concentrated by rotary evaporation to give a crude solid that was further purified by liquid chromatography on silica gel, using hexanes/dichloromethane (3/1) as eluent to afford essentially pure **35Cbz4BzCN** (1.01 g, 80%) as a light yellow solid: m.p. 308-308. ^oC; ^1H NMR (400 MHz, CD_2Cl_2) δ 8.02 (d, J = 8 Hz, 4 H), δ 7.92 (s, 2 H), δ 7.58 (d, J = 8 Hz, 2 H), δ 7.38 (t, J = 8 Hz, 2 H), δ 7.26-7.19(m, 7 H), δ 7.03 (t, J = 6.4 Hz, 1 H), δ 6.97-6.86 (m, 6 H), δ 6.65 (d, J = 8 Hz, 1 H), δ 6.43 (d, J = 8 Hz, 2 H); ^{13}C NMR (100 MHz,CD_2Cl_2): δ 144.47, 143.06, 142.23, 142.17, 141.788, 135.79, 135.67, 134.93, 133.82, 129.69, 128.91, 126.56, 126.32, 124.16, 124.08, 122.91, 121.21, 120.72, 120.27, 120.20, 117.05, 116.62, 112.338, 110.703, 110.00; MALDI calcd for $C_{44}H_{27}N_5$ ($M+1^+$) 626.2345 (100%), obsd 626.2364.

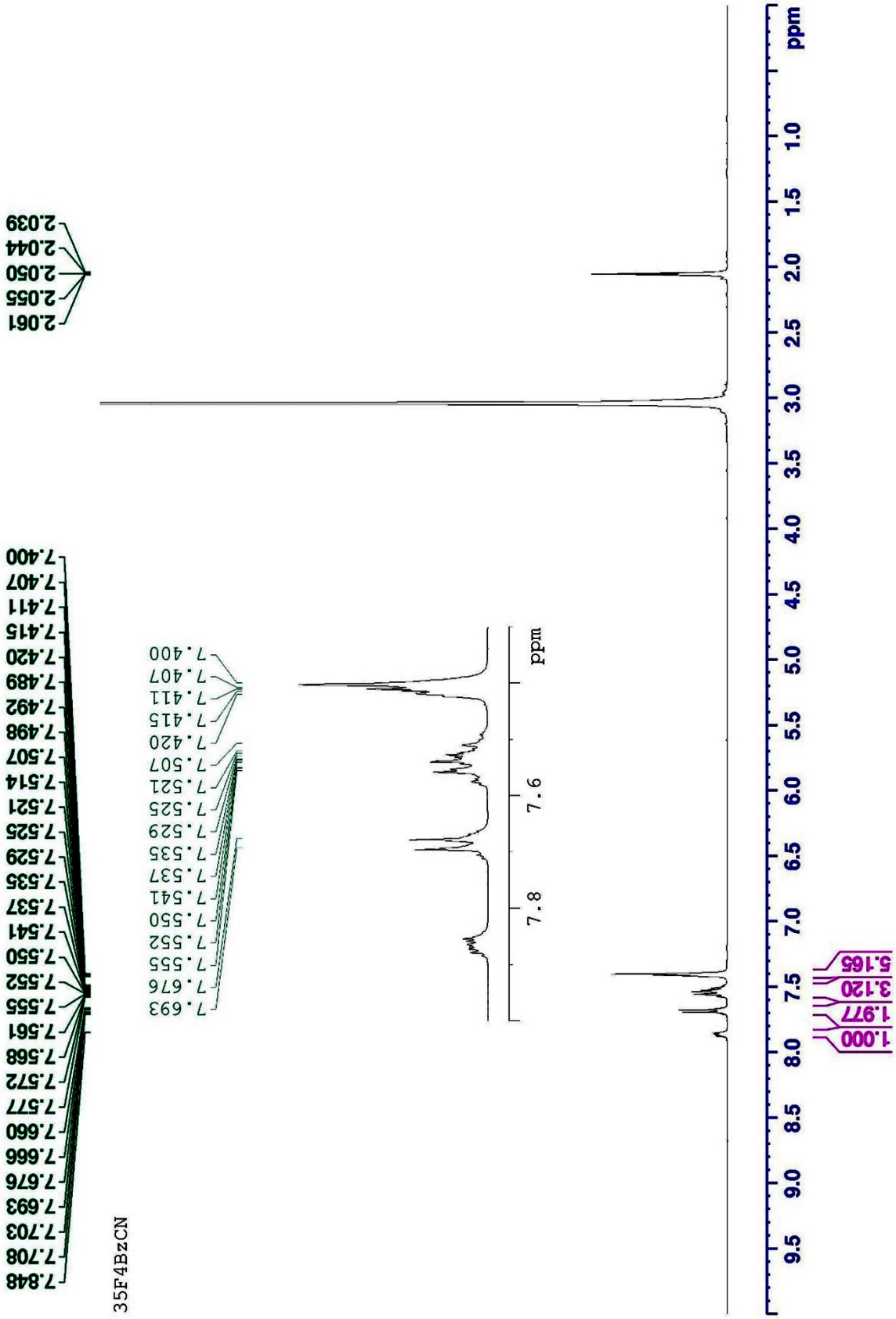

Fig. S1 ^{1}H spectrum of **35F4BzCN** in d_6-acetone

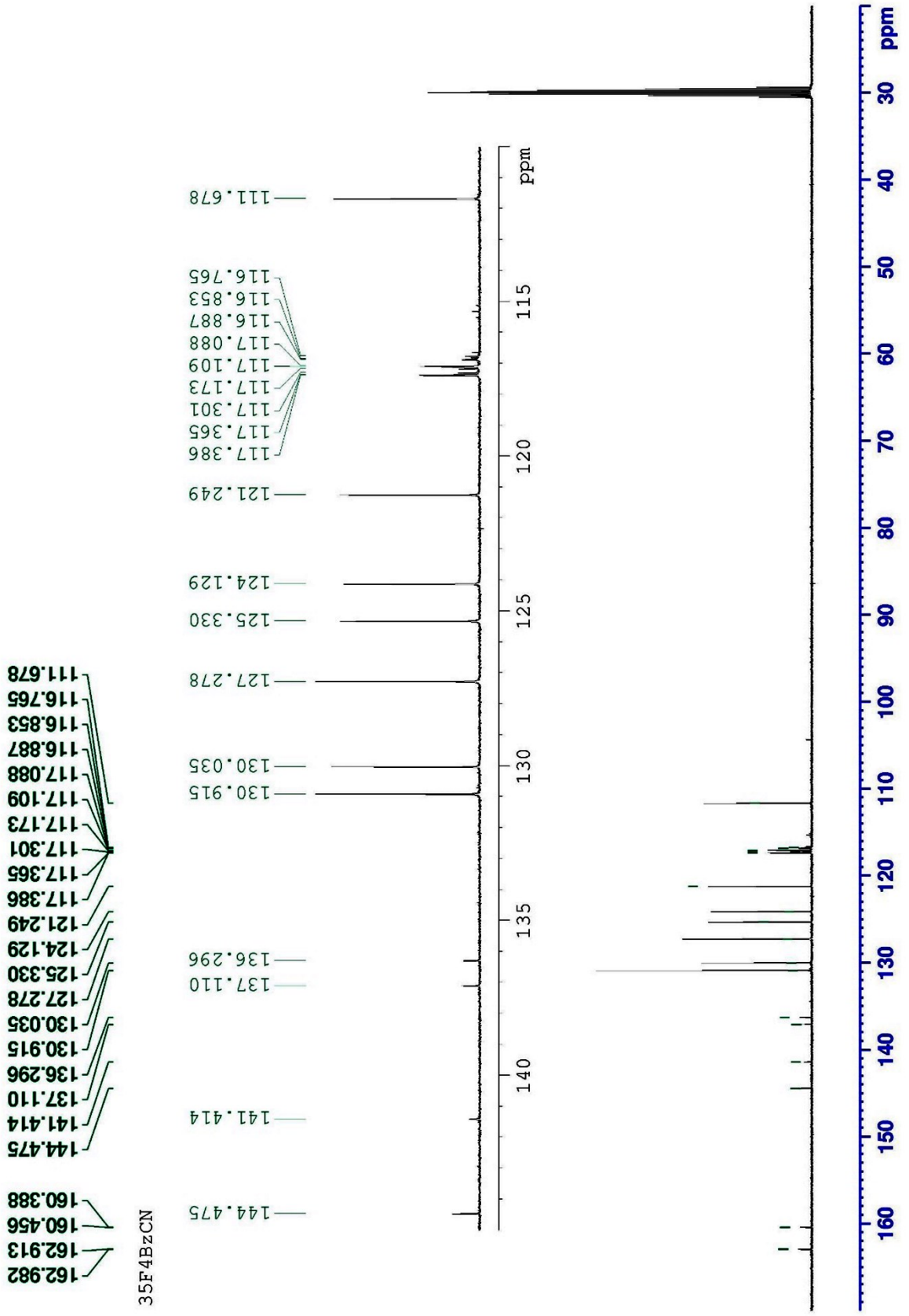

Fig. S2 ^{13}C spectrum of **35F4BzCN** in d_6-acetone

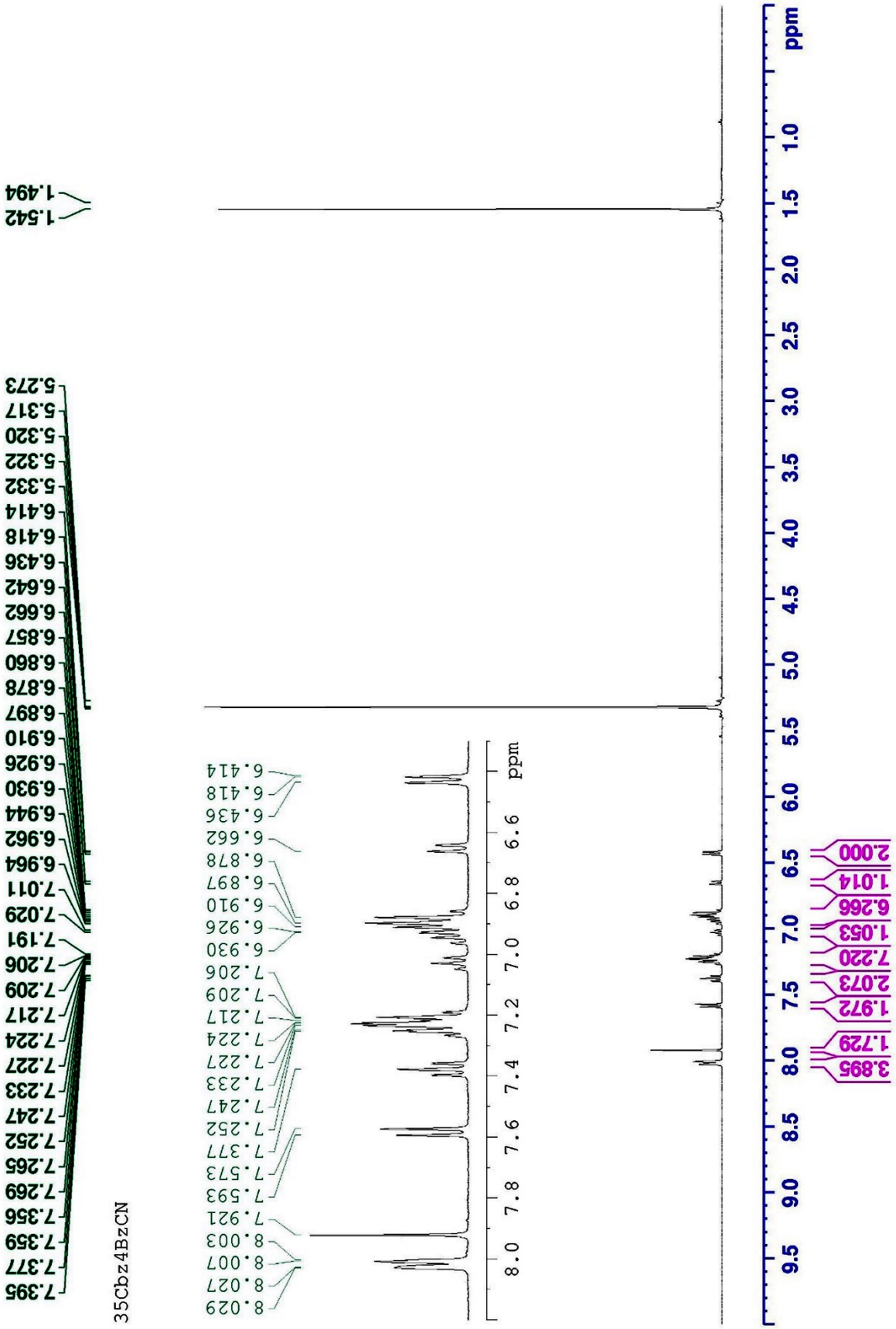

Fig. S3 ^{1}H spectrum of **35Cbz4BZCN** in CD_2Cl_2

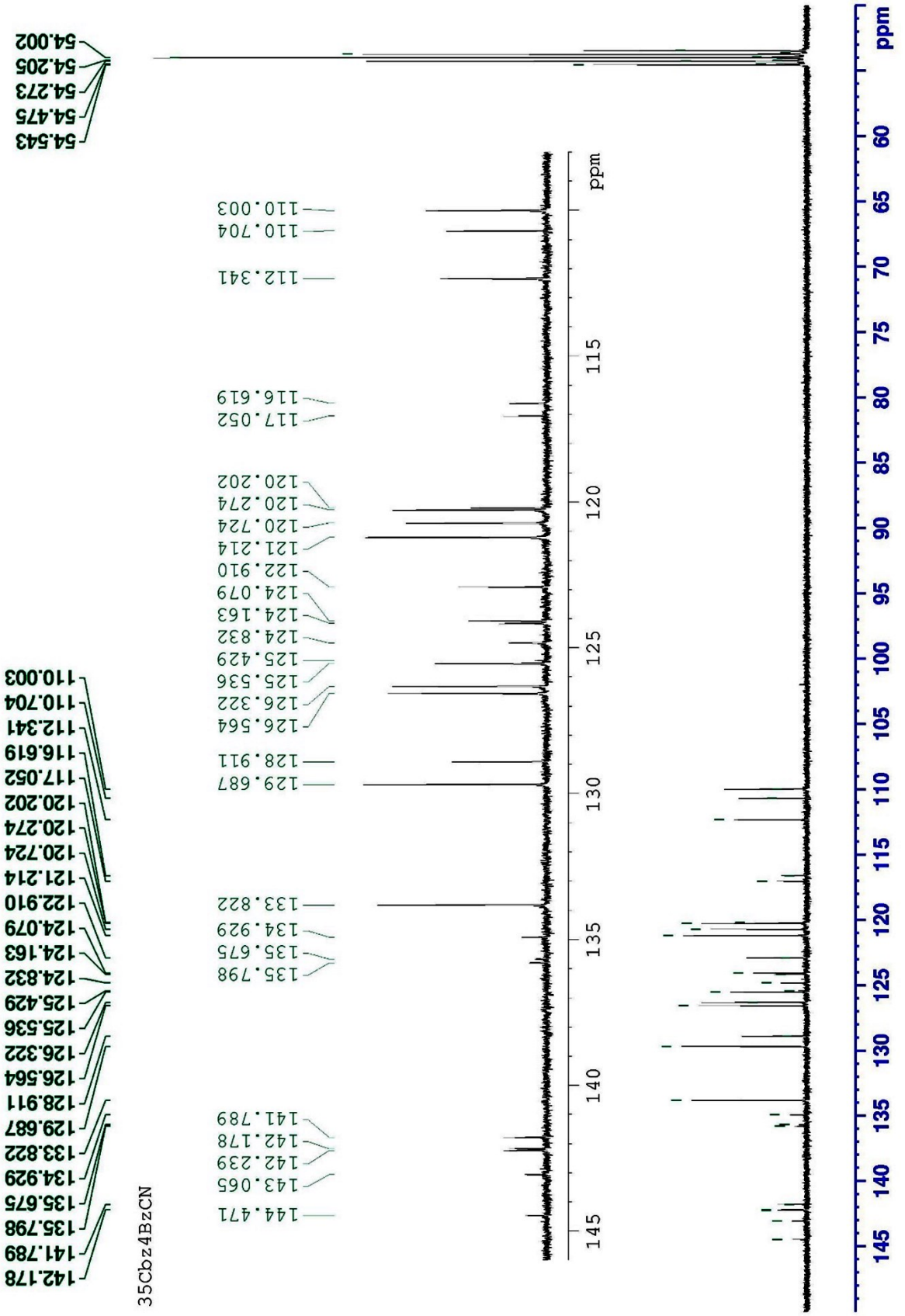

Fig. S4 ^{13}C spectrum of **35Cbz4BZCN** in CD_2Cl_2

The DSC scanning of **35Cbz4BzCN:**

In the first round of the DSC scan, the sample was heated to the desired temperature at a heating rate of 10.0 °C/min The temperature was then held at 350°C for 1 minute to ensure that the compound was entirely melted. The sample was then cooled back to 30.0 °C with a cooling rate of 10.0 °C/min. In the second and third repeated rounds, a heating rate of 10°C/min has been adopted.

The TGA scanning of **35Cbz4BzCN.**

The temperature was preheated to 105°C for 5 minutes, with a heating rate of 10.0°C/min, and then heated to 800°C at a heating rate of 10.0 °C/min under nitrogen atmosphere.

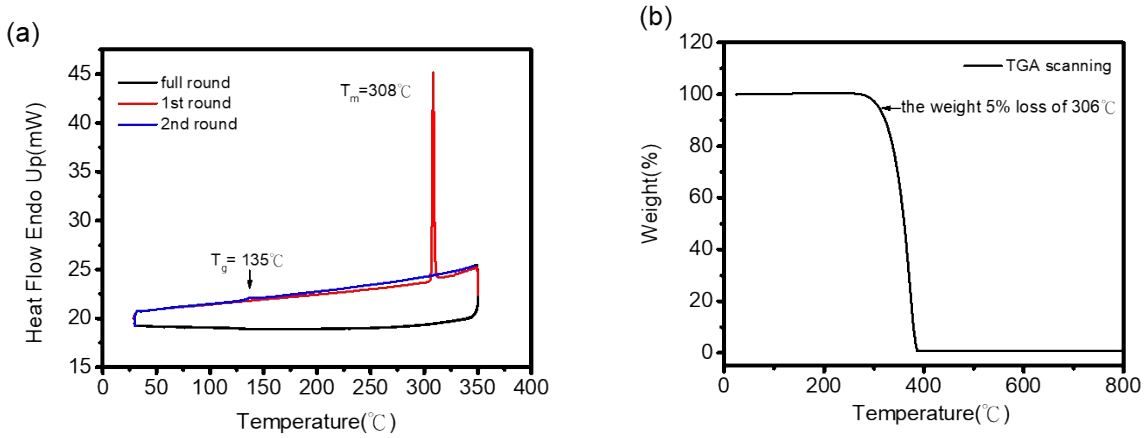

Fig. S5 (a) DSC measurement of **35Cbz4BzCN** and (b) TGA scanning of **35Cbz4BzCN**.

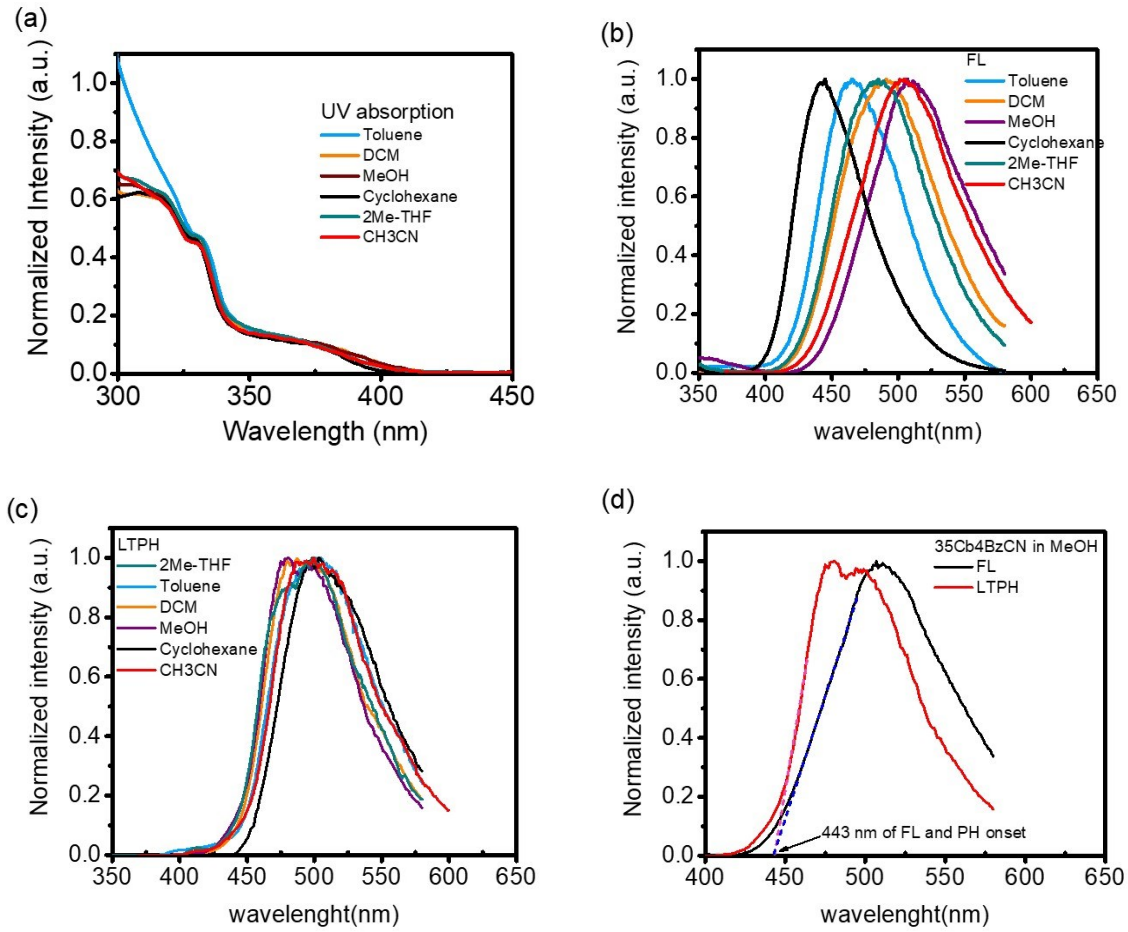

Fig. S6 Solvatochromic shifts of **35Cbz4BzCN** in various solvents: (a) UV absorption; (b) fluorescence spectra; (c) phosphorescence spectra; (d) Comparison of the fluorescence and phosphorescence in MeOH.

Photophysical measurements

Steady-state absorption and emission spectra in both solution and solid were recorded with a Hitachi (U-3310) spectrophotometer and an Edinburgh (FS-920) fluorimeter, respectively. Solid-state emission quantum yields were determined by the Jobin-Yvon FL3-21 Horibafluorolog fluorimeter equipped with an integrated sphere. Lifetime studies were performed with an Edinburgh (FL-980) photon-counting system with a 375 nm diode laser excitation source with 40 kHz repetition rate. The time-resolved delayed photoluminescence spectra were acquired for probing the insights of the emissive properties. At zero delay time and a gate width of 100 ns, the prompt emission component can be acquired by an intensified charge-coupled detector equipped with an Nd:YAG 355 nm laser as excitation source, which the emission band is contributed to fluorescence, whereas the component of phosphorescence was acquired at a delay with different gate width. During the experiment, a third harmonic of a Nd:YAG laser (Continuum, Surelite) at 355 nm was used as the pump pulse, which has a duration of 15 ns and a repetition rate of 10 Hz. Under this experimental conditions, collection of the phosphorescence data in the 50 μs time scale is allowed.

Besides, Zeiss LSM 710 (Zeiss, Germany) technique equipped with 80 MHz fs mode-locked Ti-Sapphire laser (Mai-Tai DeepSee, Spectra-Physics) for the two-photon excitation microscopy. In order to gather signals, Plan-Apochromat 63x/1.4 oil immersion objective lens (Zeiss, Germany) was employed. To calculate k_r and k_{nr}, the following equations are also employed:

$\tau_{obs} = \tau_1*(A_1)+ \tau_2*(A_2)$

$k_{obs} = 1/ \tau_{obs}$

$k_r=QY*k_{obs}$

$k_{obs}=k_r + k_{nr}$

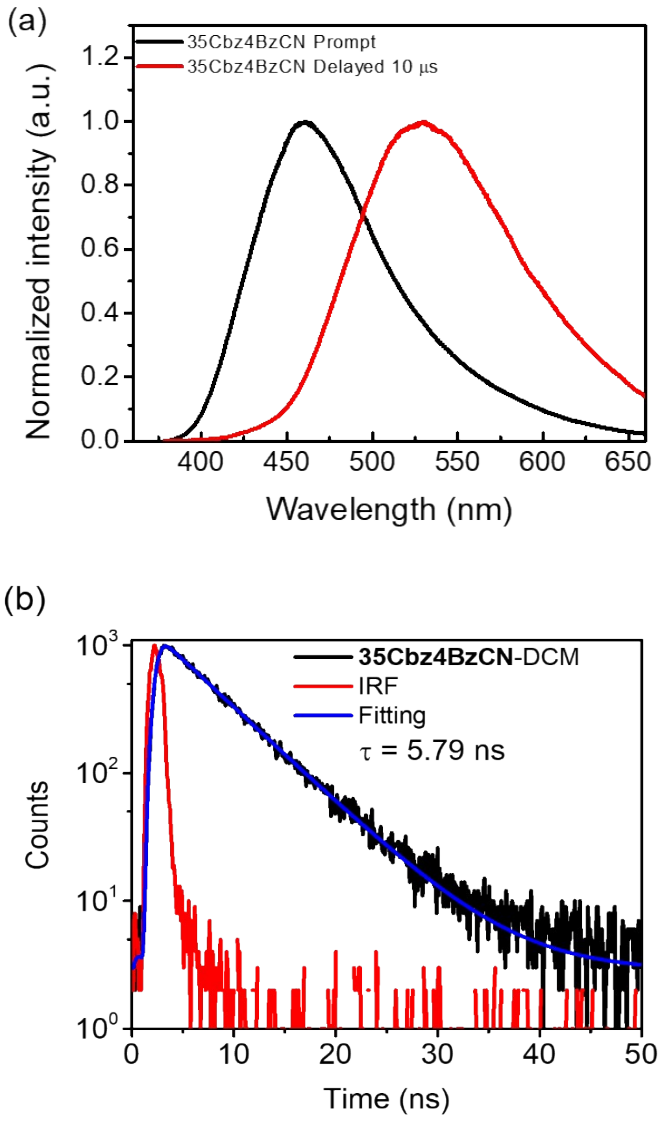

Fig. S7 (a) The prompt and delayed photoluminescence (PL) spectra of **35Cbz4BzCN** in dichloromethane at 77K. The prompt one is assigned to the fluorescence emission and the delayed one is assigned to the phosphorescence emission. (b) The prompt time resolved PL decay of **35Cbz4BzCN** in dichloromethane at 77K.

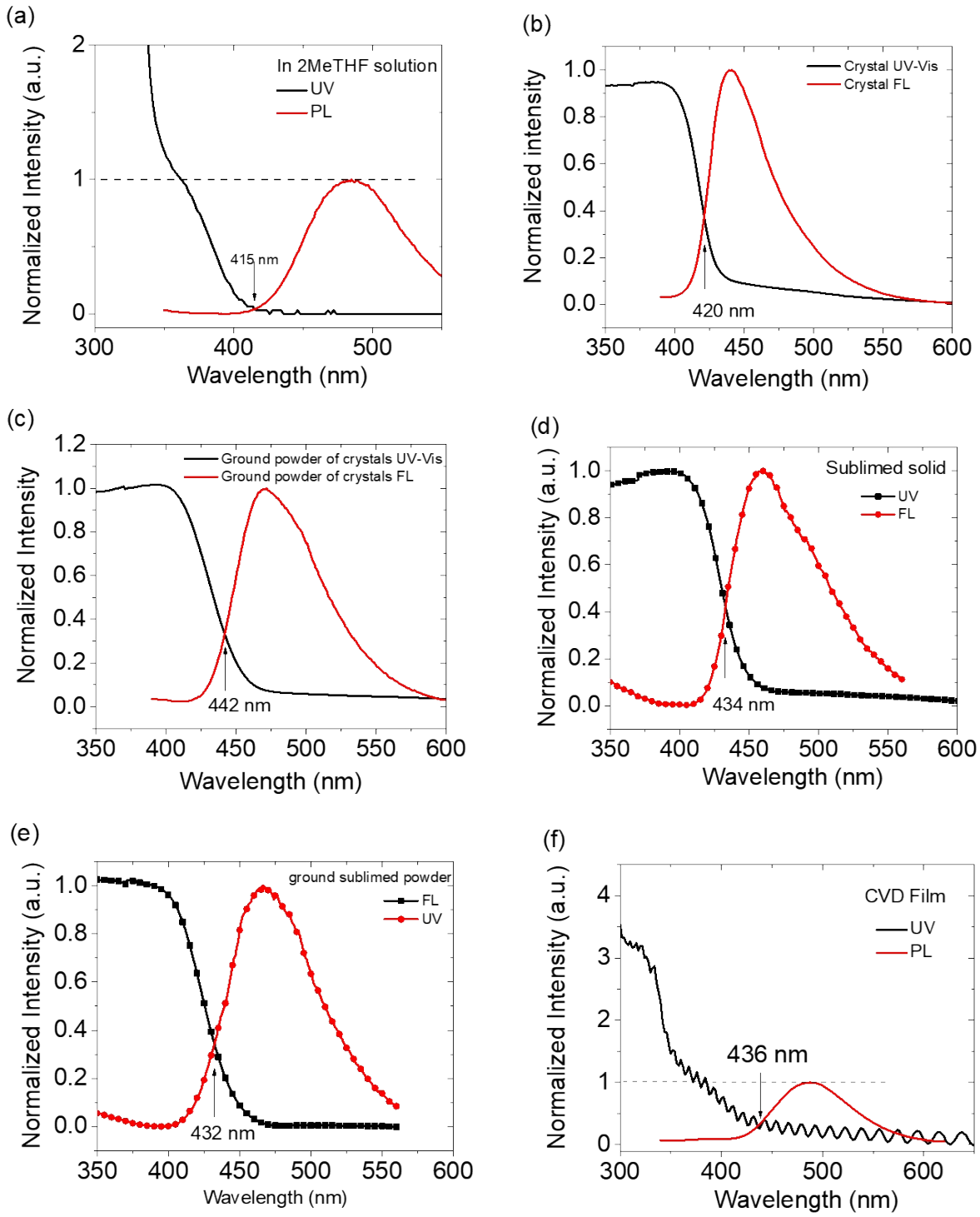

Fig. S8 The FL onset of **35Cbz4BzCN** in (a) 2MeTHF solution; (b) crystals; (c) ground powder of crystals; (d) sublimed solid; (e) ground powder of sublimed solid; (f) the CVD film.

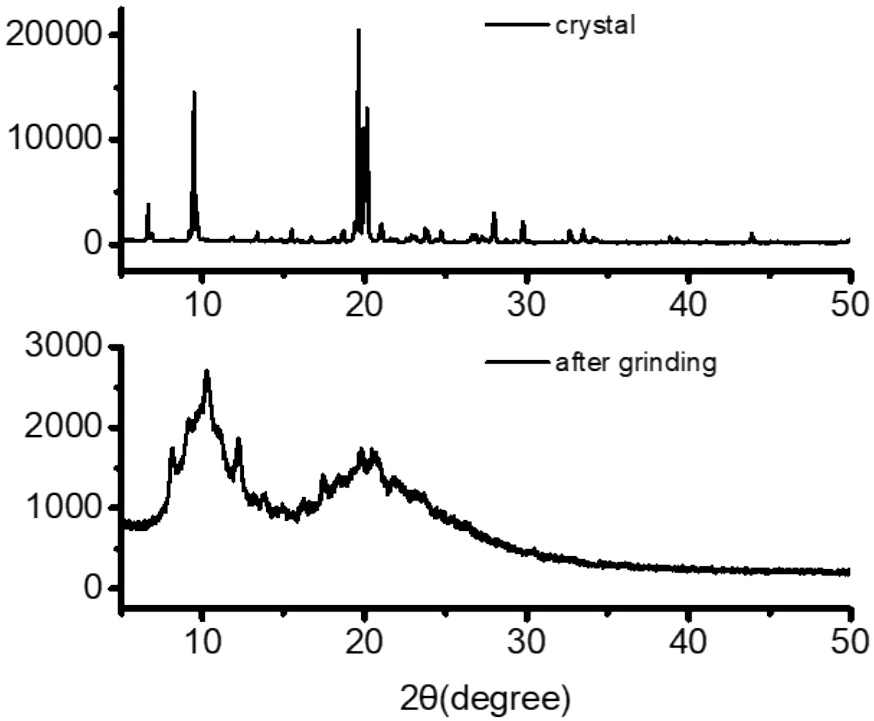

Fig. S9 (Top) Powder X-ray spectrum of the crystallines of **35Cbz4BzCN** and (bottom) powder X-ray spectrum of the ground powder of **35Cbz4BzCN** crystals. The loss of the fine diffraction pattern can clearly be observed.

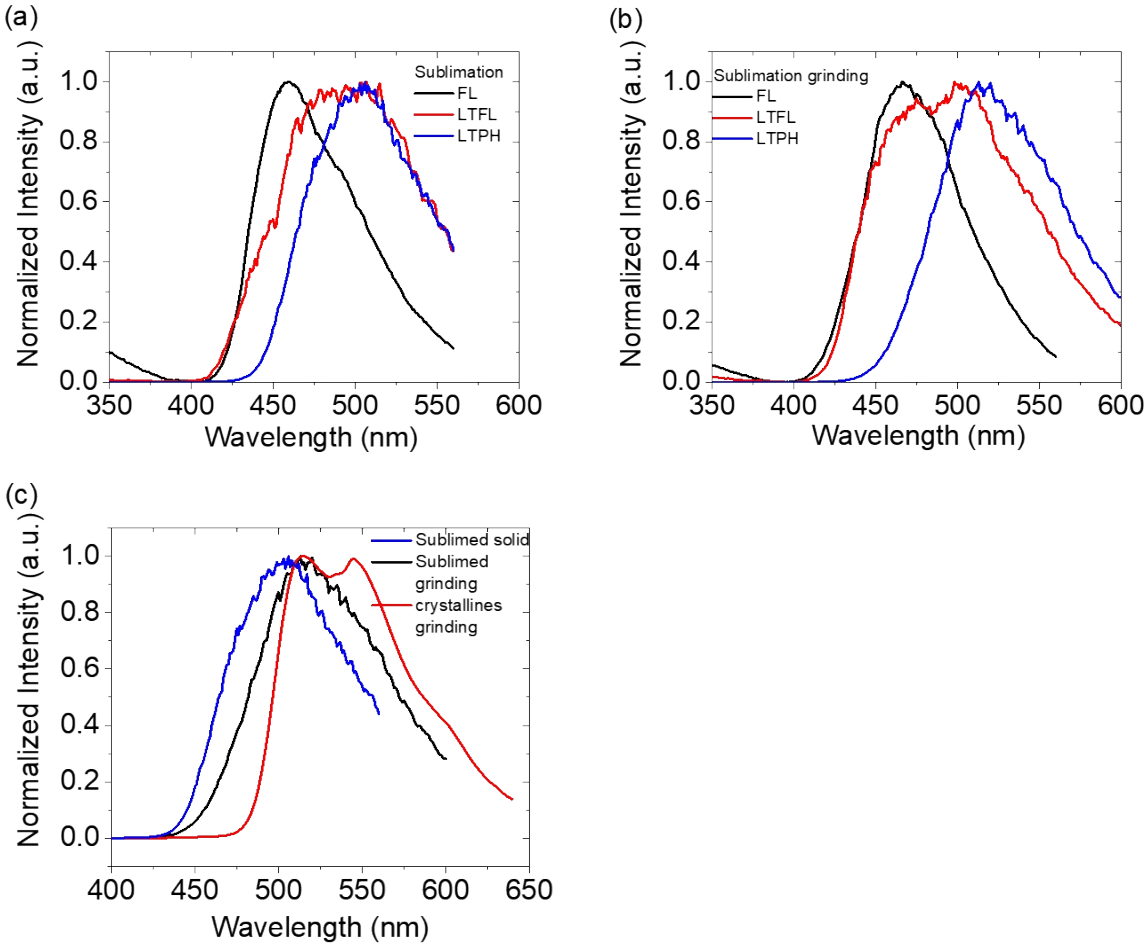

Fig. S10 The photophysical properties of (a) sublimed solid; (b) sublimed solid being ground to power; and (c) comparsion and difference of the phosphorescence between the ground powder of the crystallines and the sublimed solid of **35Cbz4BzCN** at 77 K. The red-shift mechanofluorochromic effect of the ground crystallines of **35Cbz4BzCN** is apparently more significant.

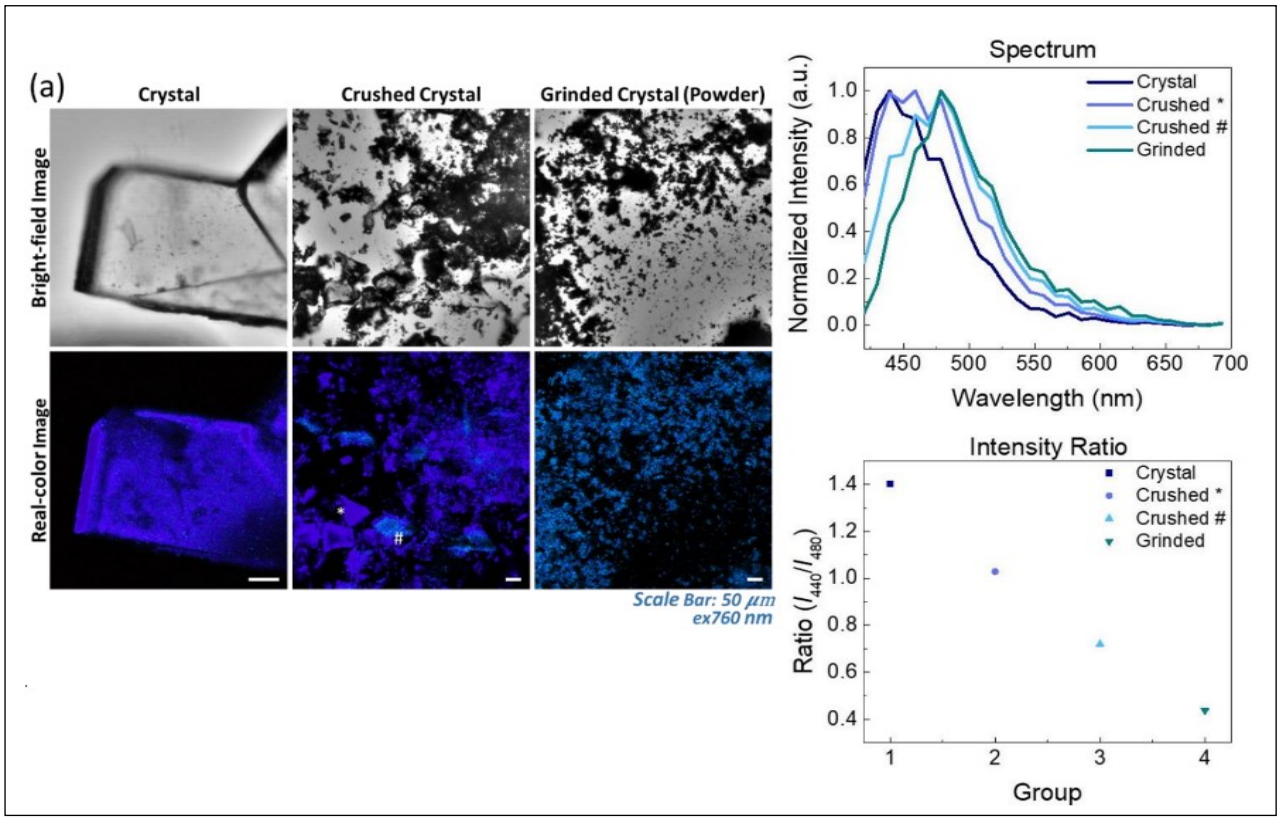

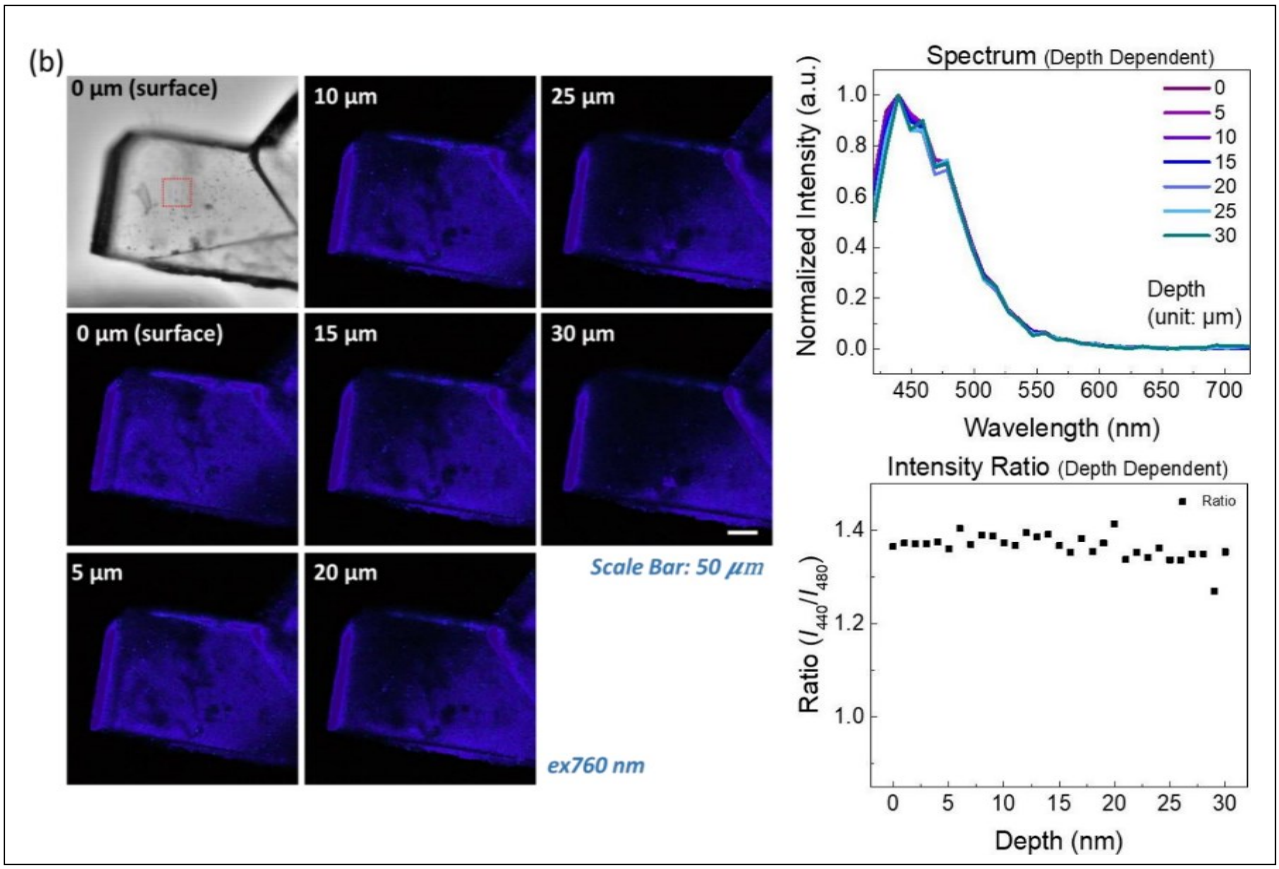

Fig S11 The two photon excitation measurements of **35Cbz4BzCN.** (a) Comparison of the emission spectra of the crystal, crushed crystal, and ground powder, and (b) measurement of the single crystal with difference excitation depth. The red shifts phenomena can still be seen.

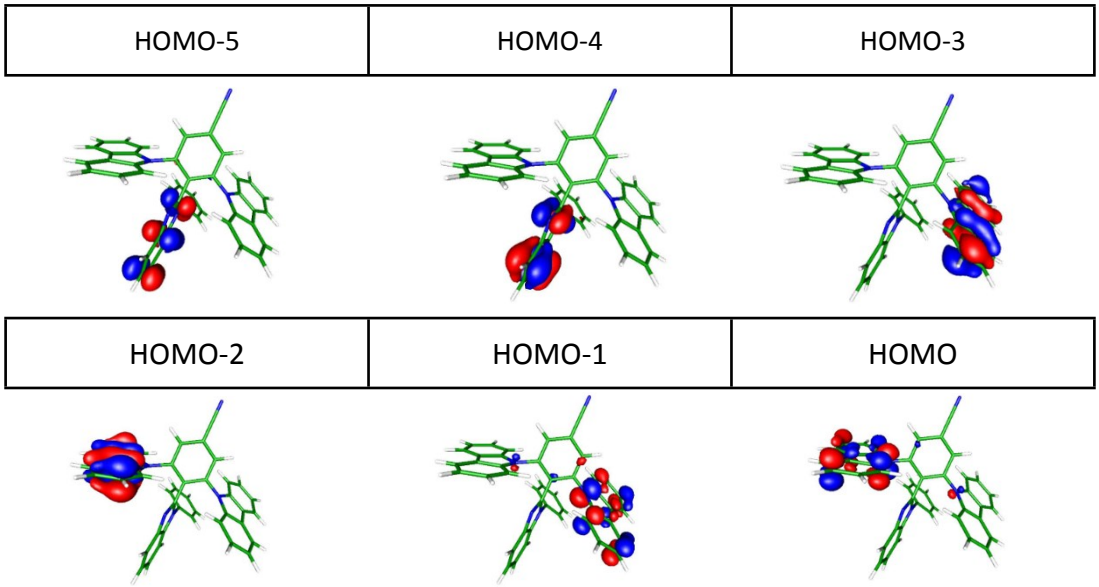

Fig. S12 The occupied MO levels for **35Cbz4BzCN** and their spatial distributions calculated by DFT.

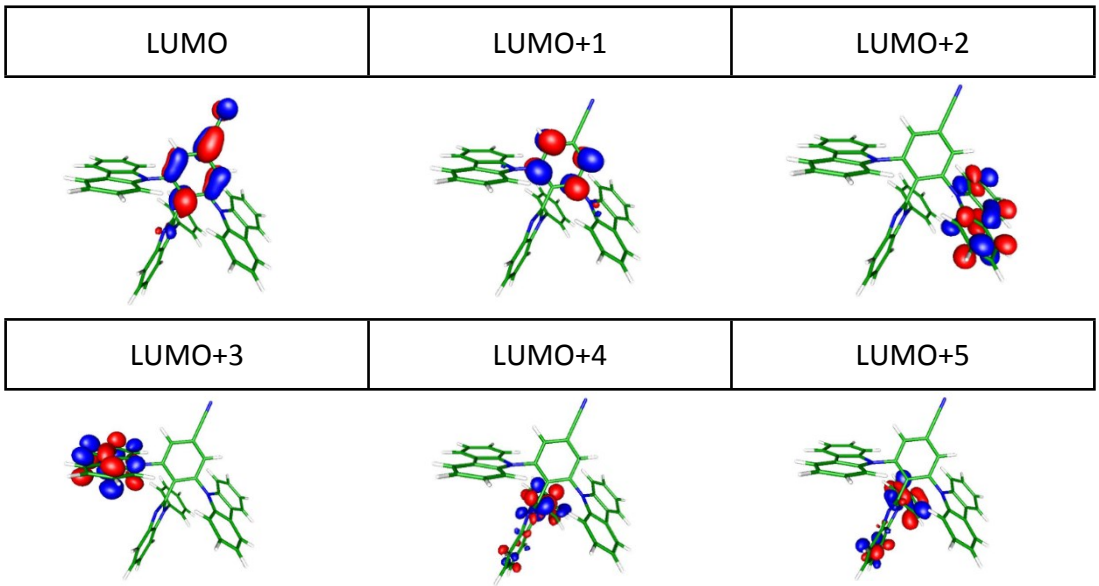

Fig. S13 The unoccupied MO levels for **35Cbz4BzCN** and their spatial distributions calculated by DFT.

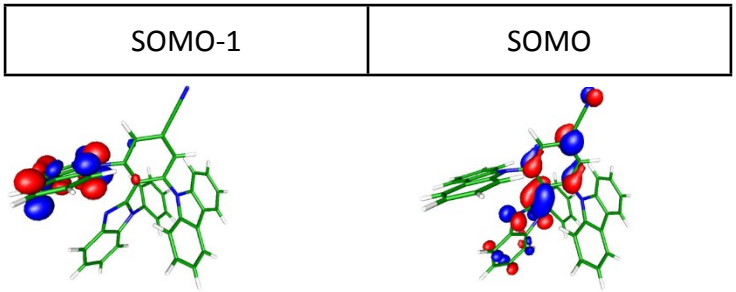

Fig. S14 The singly occupied MO levels for **35Cbz4BzCN** and their spatial distributions calculated by DFT at TD/DFT/B3LYP/6-311+g** levels.

Table S1 Calculated absorption wavelength (λ_{cal}), oscillator strength (*f*) and transition character of **35Cbz4BzCN** calculated by TD/DFT/B3LYP/6-311+g**.

λ_{cal} (nm)	*f*	Transition character (%)	assignment
431.8	0.0095	0.994078	HOMO→LUMO
411.7	0.0305	0.993345	HOMO-1→LUMO
384.89	0.0042	0.997041	HOMO-2→LUMO
373.48	0.0018	0.996844	HOMO-3→LUMO
354.14	0.0064	0.13007	HOMO-4→LUMO
		0.840249	HOMO→LUMO+1
343.96	0.0751	0.710337	HOMO-5→LUMO
		0.261726	HOMO-1→LUMO+1

Determination of the HOMO and LUMO of 35Cbz4BzCN by AC2 and Electrochemistry

The electrochemical properties of the **35Cbz4BzCN** were characterized by cyclic voltammetry (CV) and differential pulse voltammetry (DPV). Ag/AgCl was employed as a referene electrode, the Pt wire was employed as a counter electrode, and tetrabutylammonium perchlorate (0.1 M) was employed as a supporting electrolyte. The oxidation potentials were measured using a Pt working electrode in anhydrous CH_2Cl_2 (10^{-3} M), and the reduction potentials were measured with a glassy carbon working electrode in anhydrous DMF (10^{-3} M). The HOMO and LUMO values were determined according to the DPV peaks with respect to ferrocene (Fc). We compare the HOMO and LUMO energy level of **35Cbz4BzCN** and ***o*-DiCbzBz**. The cyano group effects on decreasing of the LUMO level can be clearly seen while the effects on the HOMO level is small.

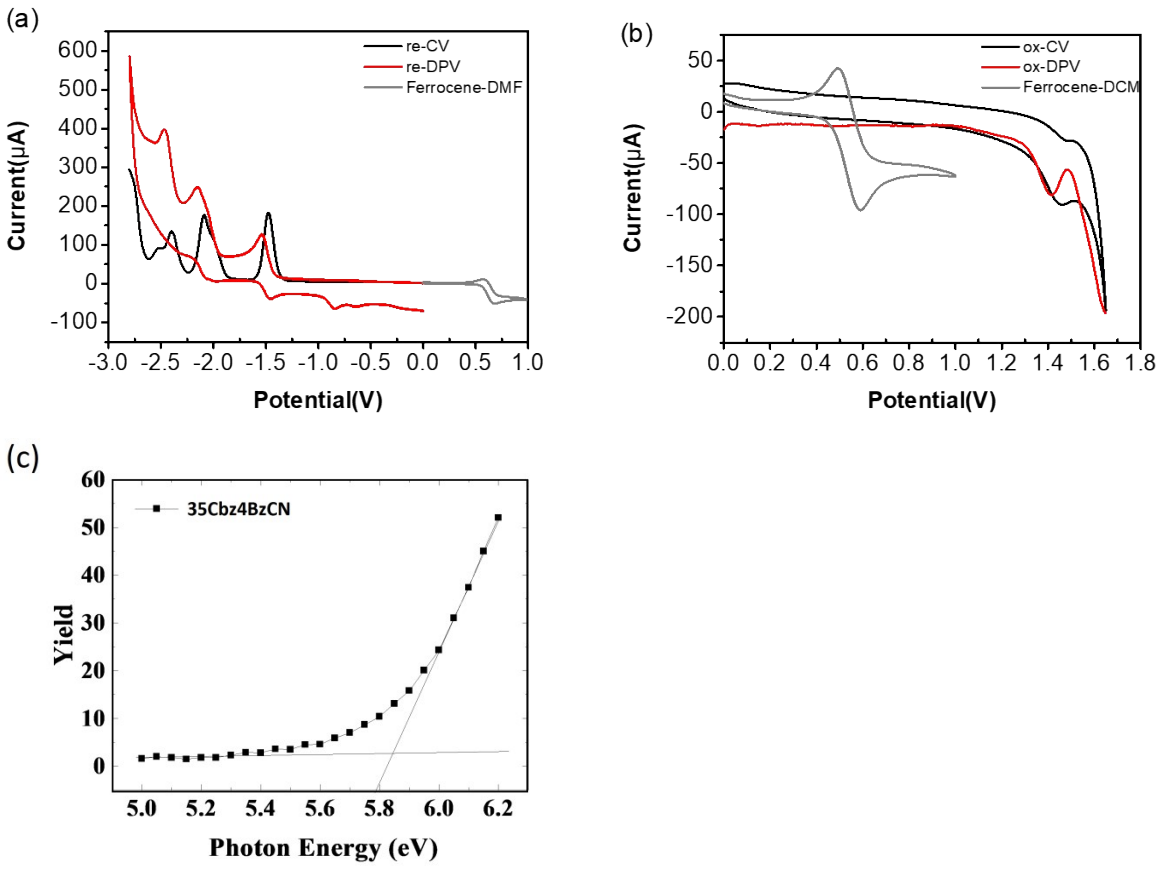

Fig. S15 CV and DPV for (a) reduction and (b) oxidation scans of **35Cbz4BzCN** and (c) AC-2 measurement.

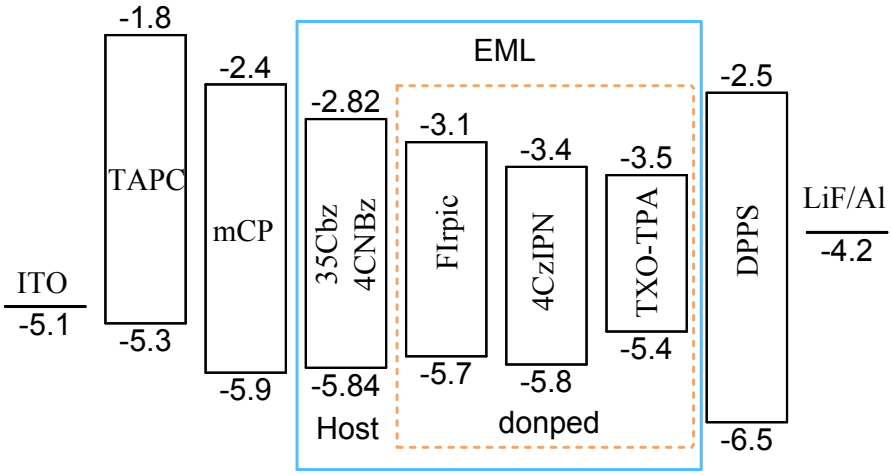

Fig. S16 HOMO and LUMO alignment of **35Cbz4BzCN** with blue, green and orange red emitters in the electroluminescence device.

35Cbz4BzCN Universal host in light emitting devices

(a) 4CzIPN as the green TADF emitter:

Dopant concentration effects.

The device structure is ITO/TAPC (50 nm)/*m*CP (10 nm)/ light emitting layer EML (V wt %) (30 nm)/DPPS (55 nm)/LiF (0.8 nm)/Al (120 nm). According this device structure, the V wt % are 1, 5 and 10 of 4CzIPN doping ratio.

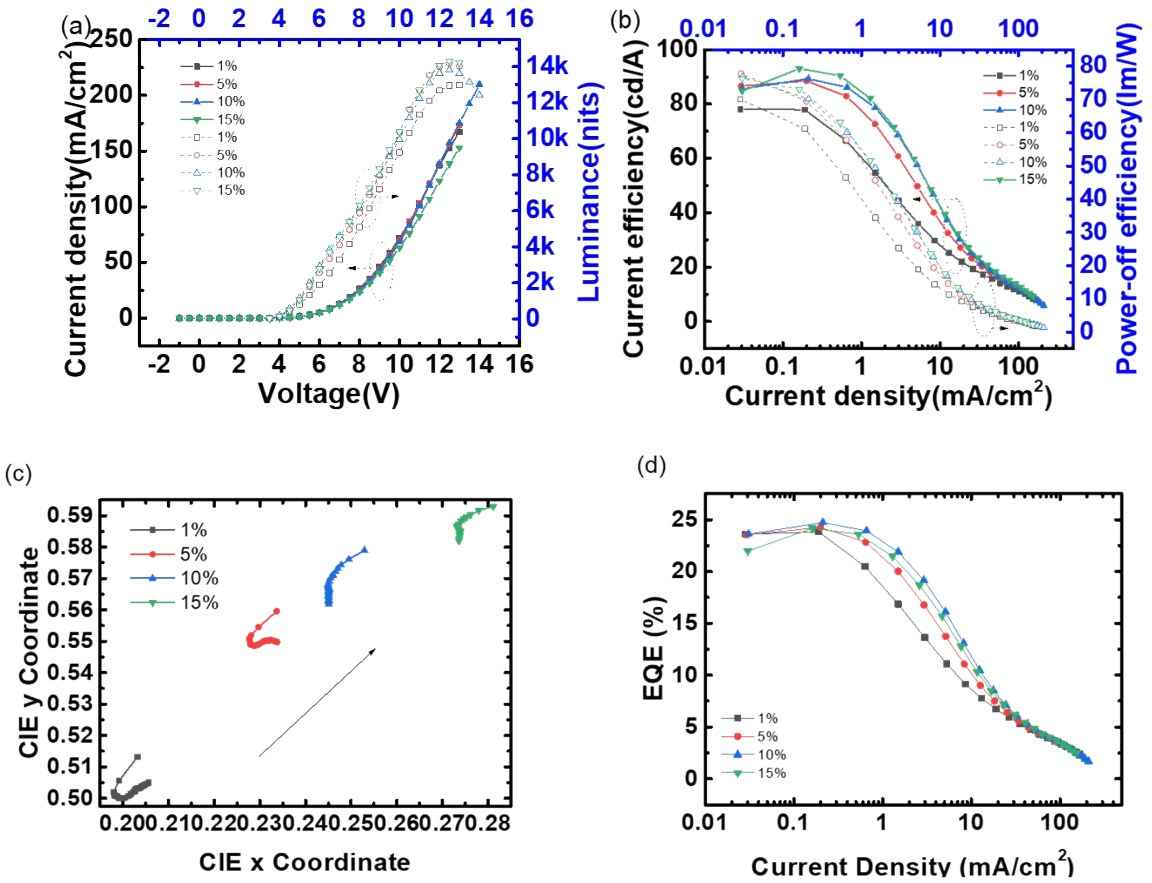

Fig. S17 Device performance of the green TADF OLED with different 4CzIPN doping ratio: (a)the J-L-V plots; (b) the current density-current efficiency-power efficiency curve; (c) CIE coordinate; (d) the current density- EQE curve

Table S2 Performance of **35Cbz4BzCN** OLED with different 4CzIPN doping ratio.

Device entry	Driving voltage (V)[a]	Max luminance (nits)	CE (cd/A)	PE (lm/W)	EQE (%)	LT50@ 1000nits (min)
1%	4.71	12980	78.1[b], 51.0[d]	70.1[c], 31.1[d]	23.6[b], 15.7[d]	16[d]
5%	4.71	14190	88.5[b],74.1 [d]	77.8[c],47.6[d]	24.3[b], 17.3[d]	10[d]
10%	4.70	13630	89.3[b],80.8 [d]	76.9[c],52.6[d]	24.7[b], 22.3[d]	13[d]
15%	4.81	14310	93,0[b],90.7 [d]	76.2[c],53.0[d]	24.2[b], 21.7[d]	12[d]

[a]: J=1mA/cm^2. [b]: At max current efficiency. [c]: At max power off efficiency. [d]: At 1000nits.

Device ETL thickness scan

The device structure is ITO/TAPC (50 nm)/*m*CP (10 nm)/EML (10 wt %) (30 nm)/DPPS (Y nm)/LiF (0.8 nm)/Al (120 nm). The Y are 55 nm, 60 nm,65 nm 70 nm and 75 nm of ETL thickness.

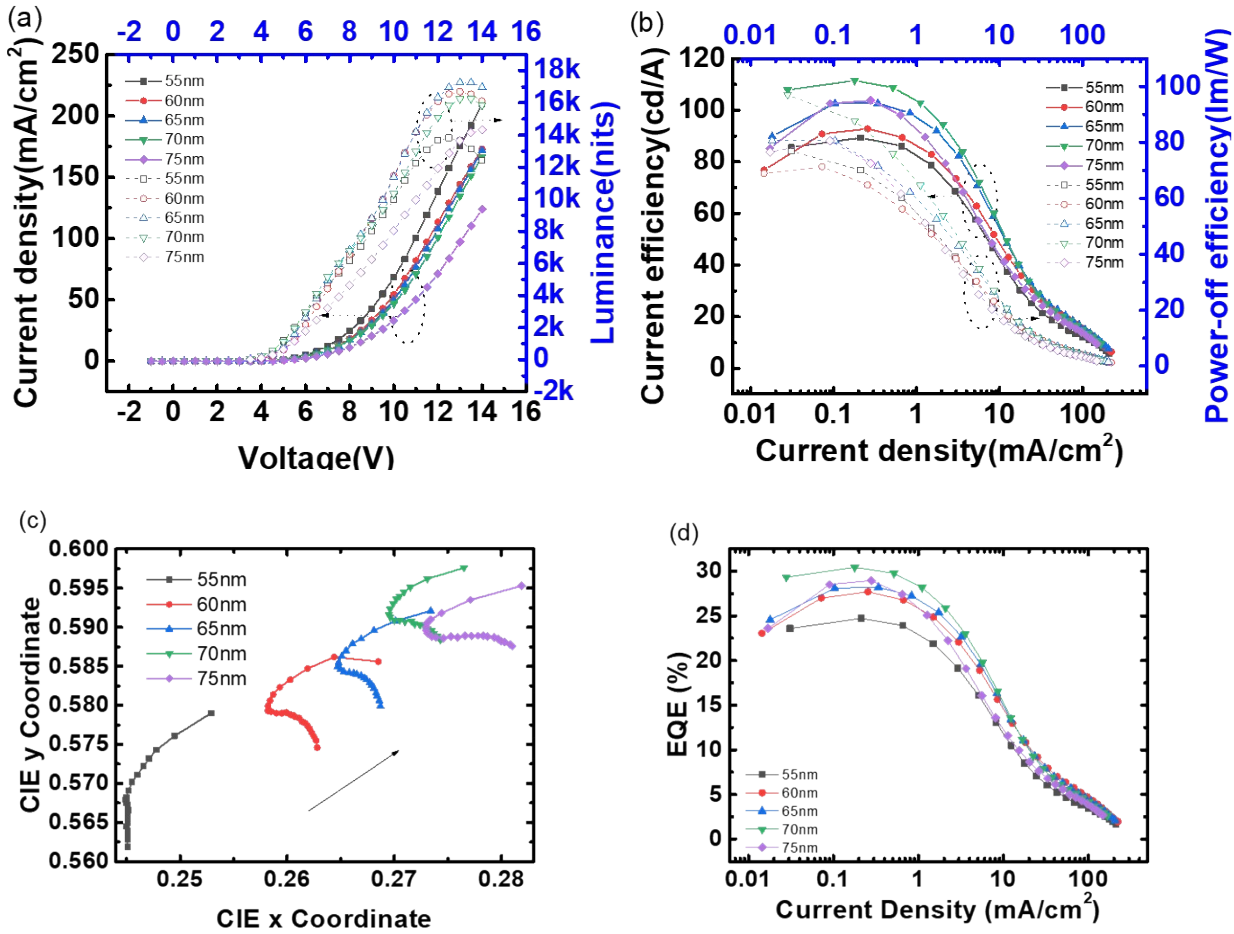

Fig. S18 Device of the green TADF OLED with different ETL thickness: (a)the J-L-V plots; (b) the current density-current efficiency-power efficiency curve; (c) CIE coordinate; (d) the current density- EQE curve.

Table S3 Performance of **35Cbz4BzCN** OLED with different ETL thickness.

Device entry	Driving voltage (V)[a]	Max luminance (nits)	CE (cd/A)	PE (lm/W)	EQE (%)	LT50@ 1000nits (min)
55nm	4.70	13630	89.3[b], 80.8[d]	76.9[c], 52.6[d]	24.7[b], 22.3[d]	13[d]
60nm	5.20	16700	92.8[b], 85.4[d]	71.3[c], 50.7[d]	27.7[b], 25.6[d]	25[d]
65nm	5.09	17270	102.6[b], 97.3[d]	80.7[c], 59.9[d]	28.2[b], 26.8[d]	26[d]
70nm	4.91	16240	111.5[b], 104.1[d]	97.0[c], 67.6[d]	30.4[b], 27.9[d]	20[d]
75nm	5.29	14340	103.8[b], 91.8[d]	80.6[c], 53.9[d]	29.0[b], 25.7[d]	22[d]

[a]: J=1mA/cm^2. [b]: At max current efficiency. [c]: At max power off efficiency. [d]: At 1000nits.

EML thickness scan

The device structure is ITO/TAPC (50 nm)/*m*CP (10 nm)/EML (10 wt %) (X nm)/DPPS (70 nm)/LiF (0.8 nm)/Al (120 nm). The X are 25 nm, 30 nm and 35 nm of EML thickness.

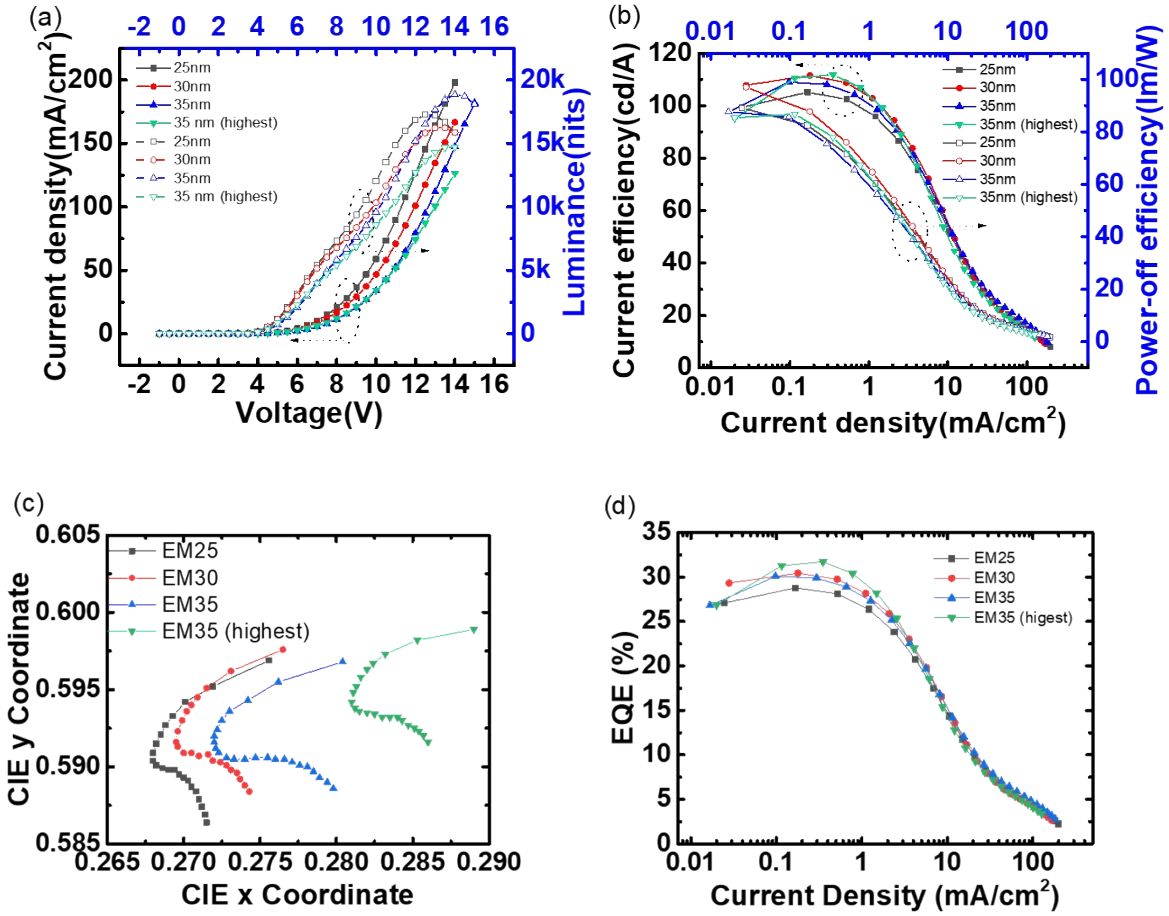

Fig. S19 Device performance of the green TADF OLED with different EML thickness: (a) the J-L-V plots; (b) the current density-current efficiency-power efficiency curve; (c) CIE coordinate; (d) the current density- EQE curve.

Table S4 Performance of **35Cbz4BzCN** OLED with different EML thickness

Device entry	Driving voltage (V)[a]	Max luminance (nits)	CE (cd/A)	PE (lm/W)	EQE (%)	LT50@ 1000nits (min)
EML25nm	4.85	17270	105.1[b], 97.4[d]	89.1[c], 63.2[d]	28.8[b], 26.2[d]	23[d]
EML30nm	4.90	16240	111.5[b],104.1[d]	97.0[c], 67.4[d]	30.4[b], 28.5[d]	20[d]
EML35nm	5.28	18860	109.0[b],101.2[d]	87.6 [c], 60.2[d]	30.1[b], 27.9[d]	28[d]
EML35nm (highest)	5.15	14730	111.8[b], 105.0[d]	86.8[c], 64.4[d]	31.7[b], 29.8[d]	17[d]

[a]: J=1mA/cm^2. [b]: At max current efficiency. [c]: At max power off efficiency. [d]: At 1000nits.

Transient electroluminescence (TrEL) characteristics of the devices

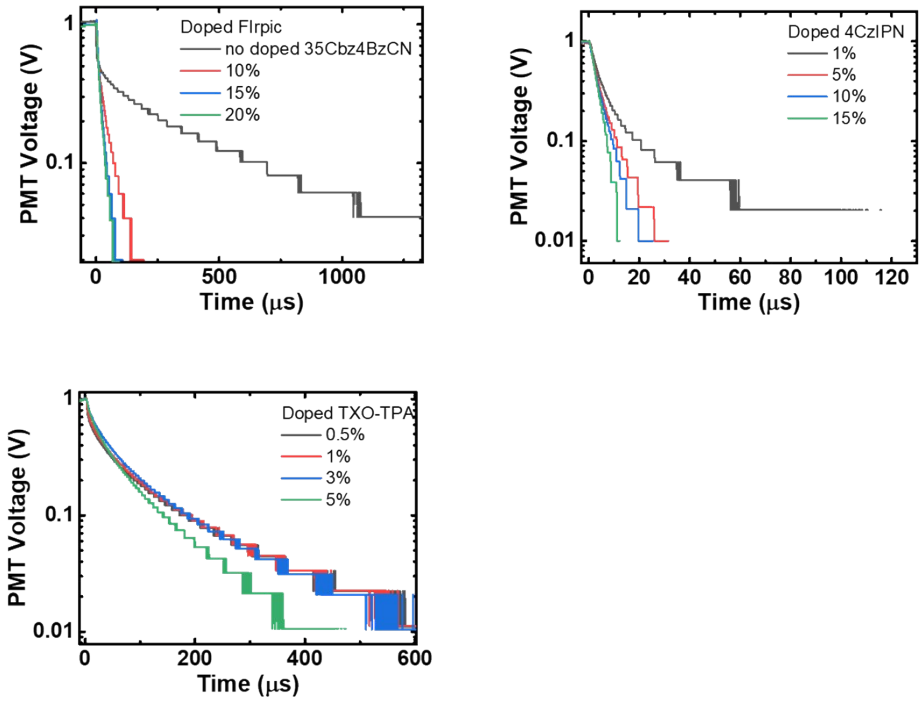

Fig. S20 Transient electroluminescence (TrEL) of the FIrpic, 4CzIPN and TXO-TPA doped OLED.

Table S5 The decay half-life time of TrEL

Device entry	A_1	τ_1	A_2	τ_2
Non-doped 35Cbz4BzCN	0.35	4.54	0.65	427
Doped FIrpic 10%	0.57	7.17	0.49	42.9
Doped FIrpic 15%	0.55	5.33	0.42	21.6
Doped FIrpic 20%	0.48	4.88	0.52	16.6
Doped 4CzIPN 1%	0.70	3.02	0.30	12.2
Doped 4CzIPN 5%	1	4.36	-	-
Doped 4CzIPN 10%	1	3.88	-	-
Doped 4CzIPN 15%	1	3.15	-	-
Doped TXO-TPA 0.5%	0.60	28.5	0.40	162
Doped TXO-TPA 1%	0.60	27.8	0.40	154
Doped TXO-TPA 3%	0.57	25.6	0.43	124
Doped TXO-TPA 5%	0.57	21.8	0.43	97.6

(b) 35Cbz4BzCN doped FIrpic as the blue light emitting layer (EML).

Blue phosphorescent-Concentration Scan.

The device structure is ITO/TAPC (50 nm)/*m*CP (10 nm)/EML (V wt %) (30 nm)/DPPS (55 nm)/LiF (0.8 nm)/Al (120 nm). According this device structure, the EML V are 0, 10, 15 and 20 of FIrpic doping

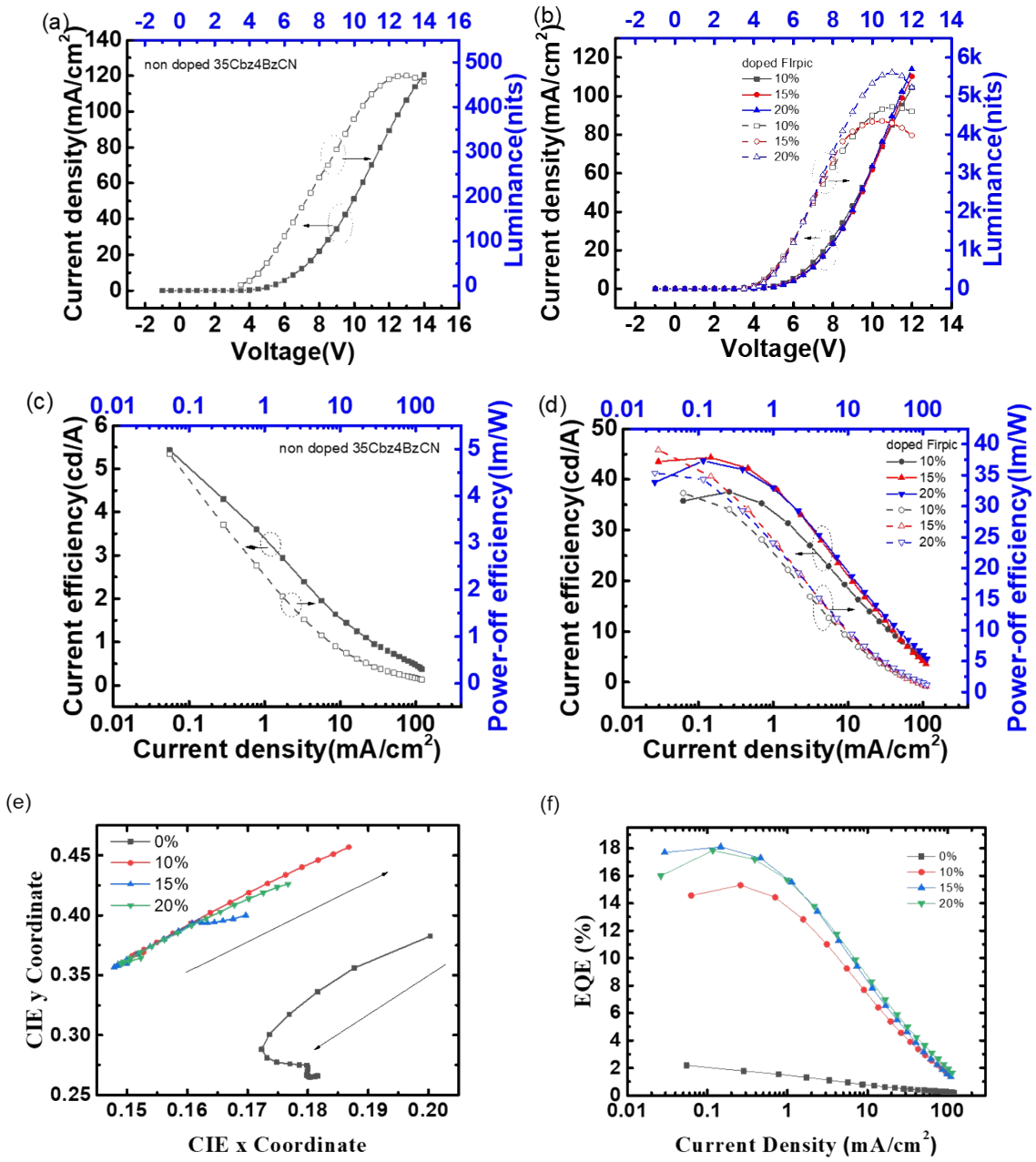

ratio.

Fig. S21 Device characteristics: The *J-L-V* plots of the blue FIrpic doped **35Cbz4BzCN** OLEDs (a) non doped; (b) with different FIrpic ratio. The current density-current efficiency-power efficiency curve of the OLEDs (c) non-doped; (d) with different FIric ratio. (e) CIE coordinate and (f) the current density- EQE curve of the OLEDs with different FIrpic ratio.

Table S6 Performance of the FIrpic doped OLED with different FIrpic dopant ratio

Device entry	Driving voltage (V) [a]	Max luminance (nits)	CE (cd/A)	PE (lm/W)	EQE (%)
Non doped 35Cbz4BzCN	4.61	470	5.4[b], 1.2[d]	4.9 [c], 1.9[d]	2.2 [b], 1.0[d]
10%	4.66	4720	37.5[b], 25.1[e]	32.1 [c], 14.0[e]	15.3 [b], 9.1[e]
15%	4.90	4360	44.3[b], 30.1[e]	39.1 [c], 16.2[e]	18.1 [b], 10.3[e]
20%	5.00	5620	43.7 [b], 30.0[e]	35.4 [c], 16.2[e]	17.8 [b], 10.6[e]

[a]: J=1mA/cm^2. [b]: At max current efficiency. [c]: At max power off efficiency. [d]: At 100 nits. [e]: At 1000 nits.

Blue phosphorescent ETL thickness scan.

The device structure is ITO/TAPC (55 nm)/*m*CP (10 nm)/EML (20 wt %) (30 nm)/DPPS (Y nm)/LiF (0.8 nm)/Al (120 nm). The Y are 55 nm, 60 nm,65 nm and 70 nm of ETL thickness.

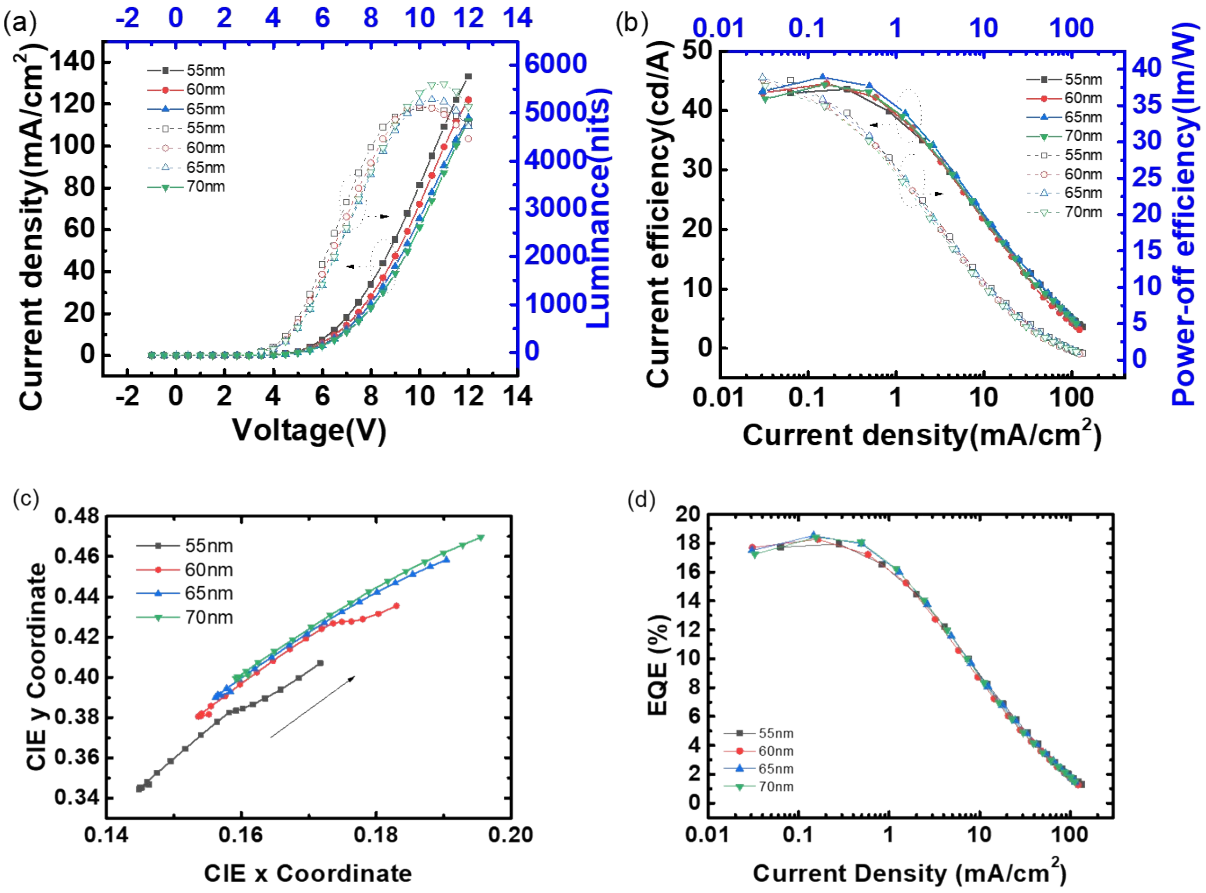

Fig. S22 ETL thickness effects on the performance of the blue FIrpic doped OLEDs: (a)the J-L-V plots; (b) the current density-current efficiency-power efficiency curve; (c) CIE coordinate; (d) the current density- EQE curve.

Table S7 ETL thickness effects on the performance of the blue FIrpic doped OLEDs

Device entry	Driving voltage (V)[a]	Max luminance (nits)	CE (cd/A)	PE (lm/W)	EQE (%)	LT50@ 1000nits (min)
55nm	4.56	5110	43.6[b], 31.8[d]	38.5[c], 19.0[d]	18.0[b], 13.1[d]	32[d]
60nm	4.71	5160	44.5[b], 32.3[d]	38.6[c], 18.8[d]	18.3[b], 13.1[d]	13[d]
65nm	4.81	5290	45.6[b], 33.2[d]	38.9[c], 18.7[d]	18.5[b], 13.3[d]	23[d]
70nm	4.86	5610	44.4[b], 33.3[d]	37.7[c], 18.8[d]	18.4[b], 13.7[d]	18[d]

[a]: J=1mA/cm^2. [b]: At max current efficiency. [c]: At max power off efficiency. [d]: At 1000nits.

Blue phosphorescent The HTL thickness scan.

The device structure is ITO/TAPC (W nm)/*m*CP (10 nm)/EML (20 wt %) (30 nm)/DPPS (65 nm)/LiF (0.8 nm)/Al (120 nm). The W are 50 nm, 55 nm and 60 nm of HTL thickness.

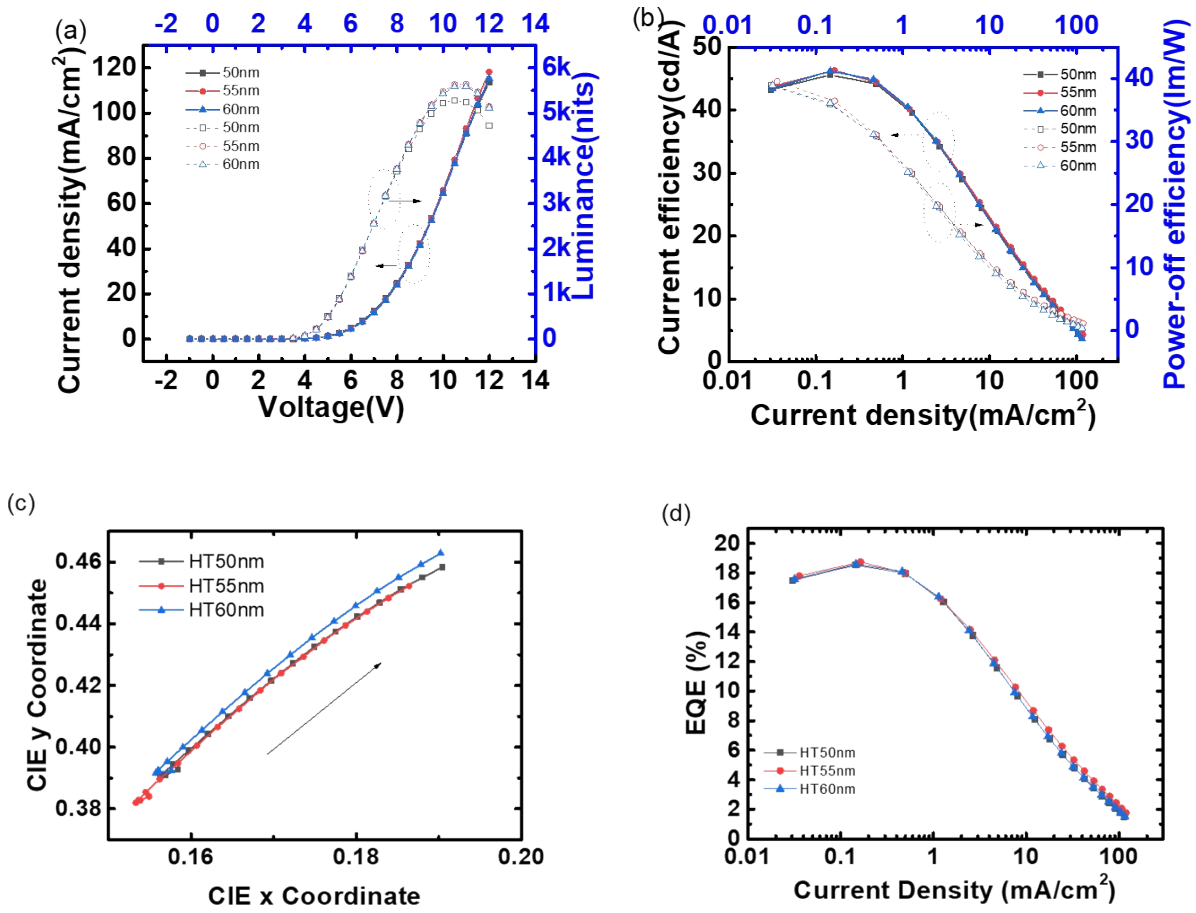

Fig. S23 HTL thickness effects on the performance of the blue FIrpic doped OLEDs: (a)the J-L-V plots; (b) the current density-current efficiency-power efficiency curve; (c) CIE coordinate; (d) the current density- EQE curve.

Table S8 HTL thickness effects on the performance of the blue FIrpic doped OLEDs

Device entry	Driving voltage (V)[a]	Max luminance (nits)	CE (cd/A)	PE (lm/W)	EQE (%)	LT50@ 1000nits (min)
50nm	4.82	5290	45.6[b], 33.2[d]	38.9[c], 18.7[d]	18.5[b], 13.3[d]	23[d]
55nm	4.85	5640	46.3[b], 33.7[d]	39.6[c], 18.9[d]	18.7[b], 13.6[d]	18[d]
60nm	4.89	5590	46.2[b], 33.7[d]	38.9[c], 18.5[d]	18.6[b], 13.5[d]	22[d]

[a]: J=1mA/cm^2. [b]: At max current efficiency. [c]: At max power off efficiency. [d]: At 1000nits.

Blue phosphorescent two host system device.

The 1 EML device structure is ITO/TAPC (55 nm)/*m*CP (10 nm)/EML (20 wt %) (30 nm)/DPPS (65 nm)/LiF (0.8 nm)/Al (120 nm), The 2 EML device structure is ITO/TAPC (55 nm)/*m*CP (10 nm)/EML(I) ***o*-diCbzBz** doped FIrpic (20 wt %) (15 nm)/ EML(II) **35Cbz4BzCN** doped FIrpic (20 wt %) (15 nm)/DPPS (65 nm)/LiF (0.8 nm)/Al (120 nm).

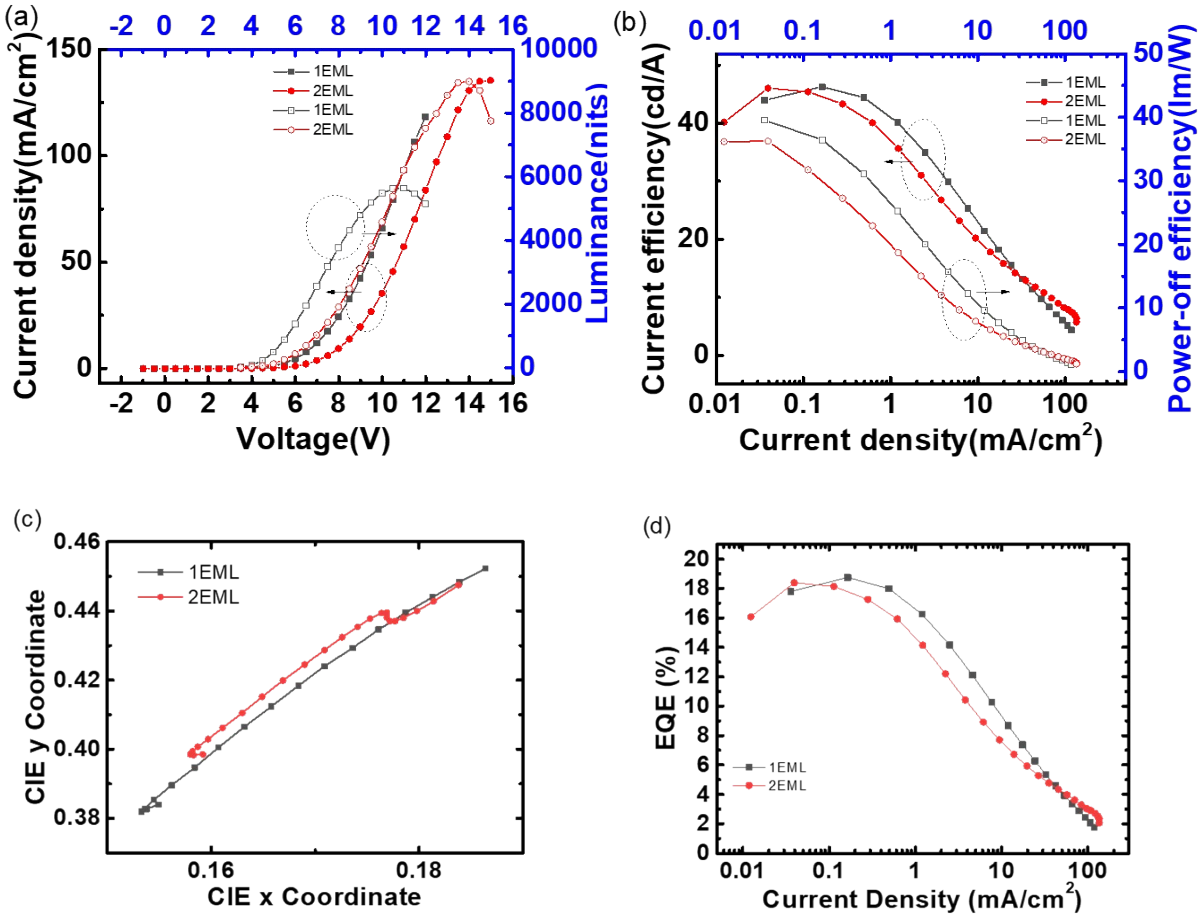

Fig. S24 Two-emitting-layer-structure effects on the performance of the blue FIrpic doped OLEDs (a) the J-L-V plots; (b) the current density-current efficiency-power efficiency curve; (c) CIE coordinate; (d) the current density- EQE curve.

Table. S9 Performance of 1EML and 2 EML OLEDs

Device entry	Driving voltage (V)[a]	Max luminance (nits)	CE (cd/A)	PE (lm/W)	EQE (%)	LT50@ 1000nits (min)
1EML	4.85	5640	46.3[b], 33.7[d]	39.6[c], 18.9[d]	18.7[b], 13.6[d]	18[d]
2EML	5.81	8990	46.1[b], 27.0[d]	36.2[c], 12.2[d]	18.4[b], 10.5[d]	11[d]

[a]: J=1mA/cm^2. [b]: At max current efficiency. [c]: At max power off efficiency. [d]: At 1000nits.

(c) 35Cbz4BzCN doped TXO-TPA as the red-light emitting layer (EML).

Red TADF Conc. Scan.

The device structure is ITO/TAPC (50 nm)/mCP (10 nm)/EML (V wt %) (30 nm)/DPPS (70 nm)/LiF (0.8 nm)/Al (120 nm). According this device structure, the EML V are 1, 5 and 10 of TXO-TPA doping ratio.

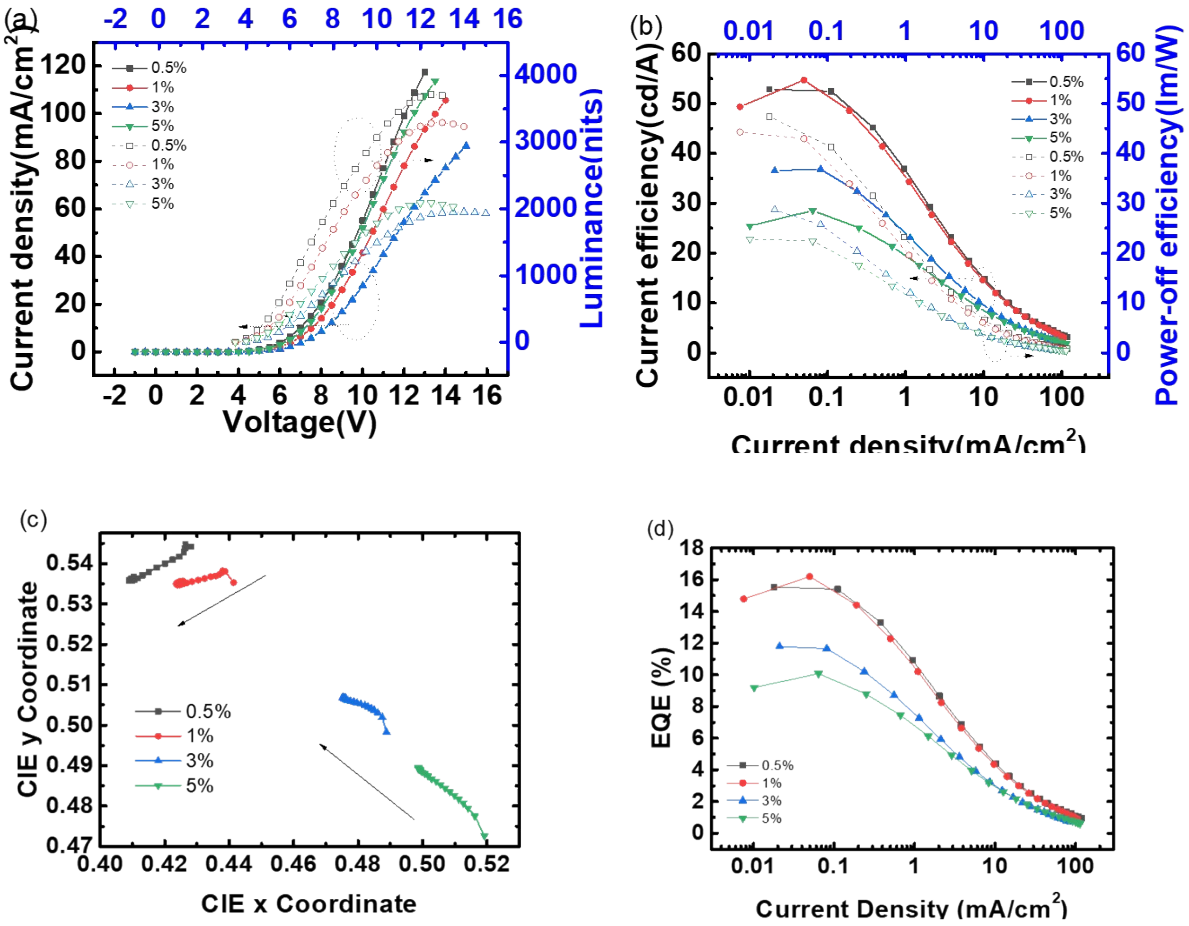

Fig. S25 TXO-TPA dopant concentration effects on the performance of the red OLEDs (a) the J-L-V plots; (b) the current density-current efficiency-power efficiency curve; (c) CIE coordinate; (d) the current density- EQE curve.

Table S10 TXO-TPA dopant concentration effects on the performance of the red OLEDs

Device entry	Driving Voltage (V)[a]	Max luminance (nits)	CE (cd/A)	PE (lm/W)	EQE (%)	LT50@ 1000nits (min)
TXO-TPA 0.5%	5.02	3710	52.8[b], 21.3[d]	47.4[c], 10.9[d]	15.5[b], 6.4[d]	26[d]
TXO-TPA 1%	5.41	3300	54.7[b], 19.2[d]	44.3[c], 9.3[d]	16.2[b], 5.9[d]	22[d]
TXO-TPA 3%	5.88	1950	36.8[b], 9.1[d]	28.7[c],3.4[d]	11.8[b], 2.9[d]	17[d]
TXO-TPA 5%	5.20	2090	28.6[b], 7.3[d]	22.8[c],3.0[d]	10.0[b], 2.5[d]	13[d]

[a]: J=1mA/cm^2. [b]: At max current efficiency. [c]: At max power off efficiency. [d]: At 1000nits.

The device ETL thickness scan.

The device structure is ITO/TAPC (50 nm)/mCP (10 nm)/EML (1 wt %) (30 nm)/DPPS (Y nm)/LiF (0.8 nm)/Al (120 nm). The Y are 70 nm, 75 nm and 80 nm of ETL thickness.

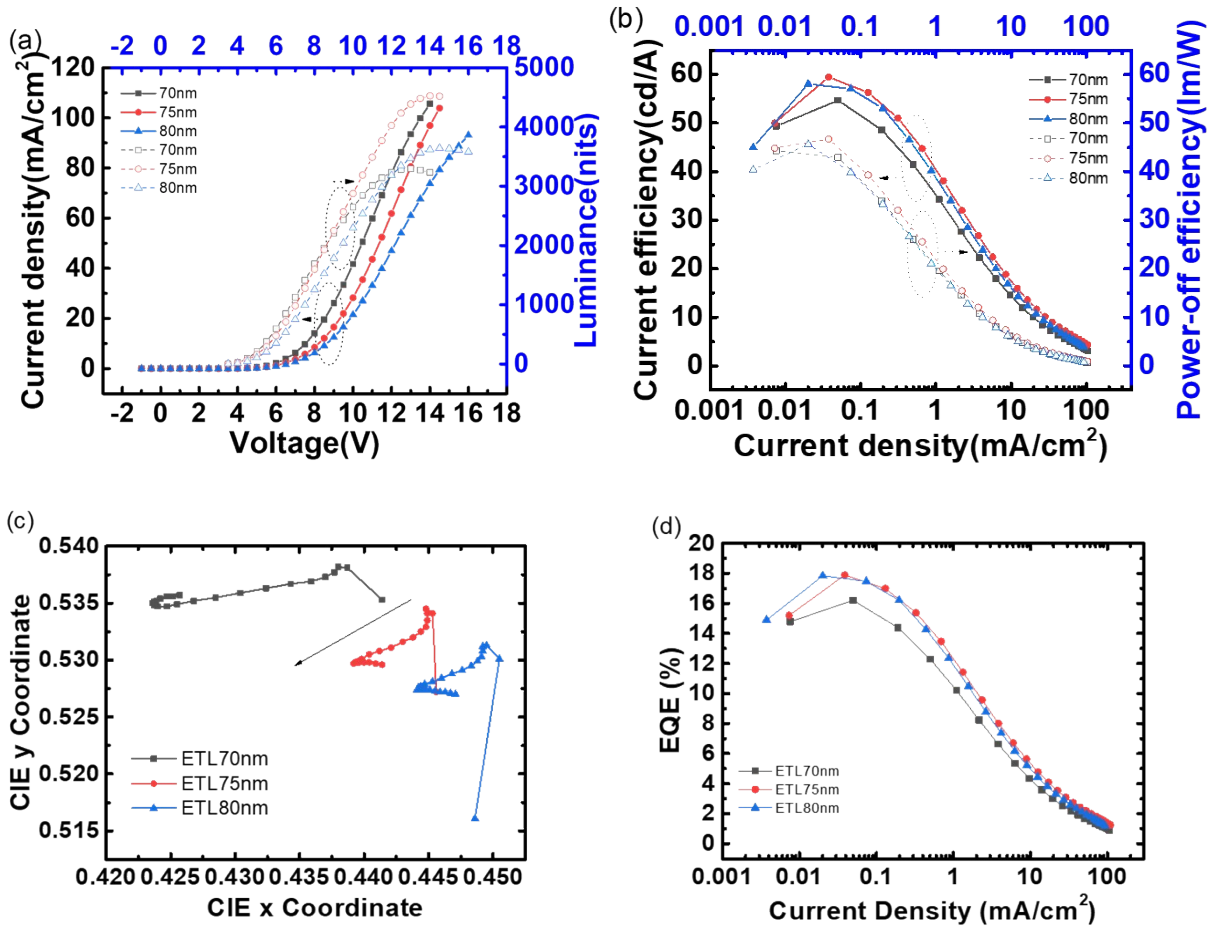

Fig. S26 ETL thickness effects on the performance of the red TXO-TPA doped OLEDs (a) the J-L-V plots; (b) the current density-current efficiency-power efficiency curve; (c) CIE coordinate; (d) the current density- EQE curve.

Table S11 ETL thickness effects on the performance of the red TXO-TPA doped OLEDs

Device entry	Driving Voltage (V)[a]	Max luminance (nits)	CE (cd/A)	PE (lm/W)	EQE (%)	LT50@ 1000nits (min)
70nm	5.41	3300	54.7[b], 19.2[d]	44.3[c], 9.3[d]	16.2[b], 5.9[d]	22[d]
75nm	5.79	4530	59.5[b], 26.5[d]	46.7[c], 11.9[d]	17.9[b], 7.9[d]	33[d]
80nm	6.09	3640	58.1[b], 23.8[d]	45.6[c],10.0[d]	17.8[b], 7.4[d]	38[d]

[a]: J=1mA/cm^2. [b]: At max current efficiency. [c]: At max power off efficiency. [d]: At 1000nits.

The device EML thickness scan.

The device structure is ITO/TAPC (50 nm)/mCP (10 nm)/EML (1 wt %) (X nm)/DPPS (75 nm)/LiF (0.8 nm)/Al (120 nm). The X are 25 nm, 30 nm and 35 nm of EML thickness.

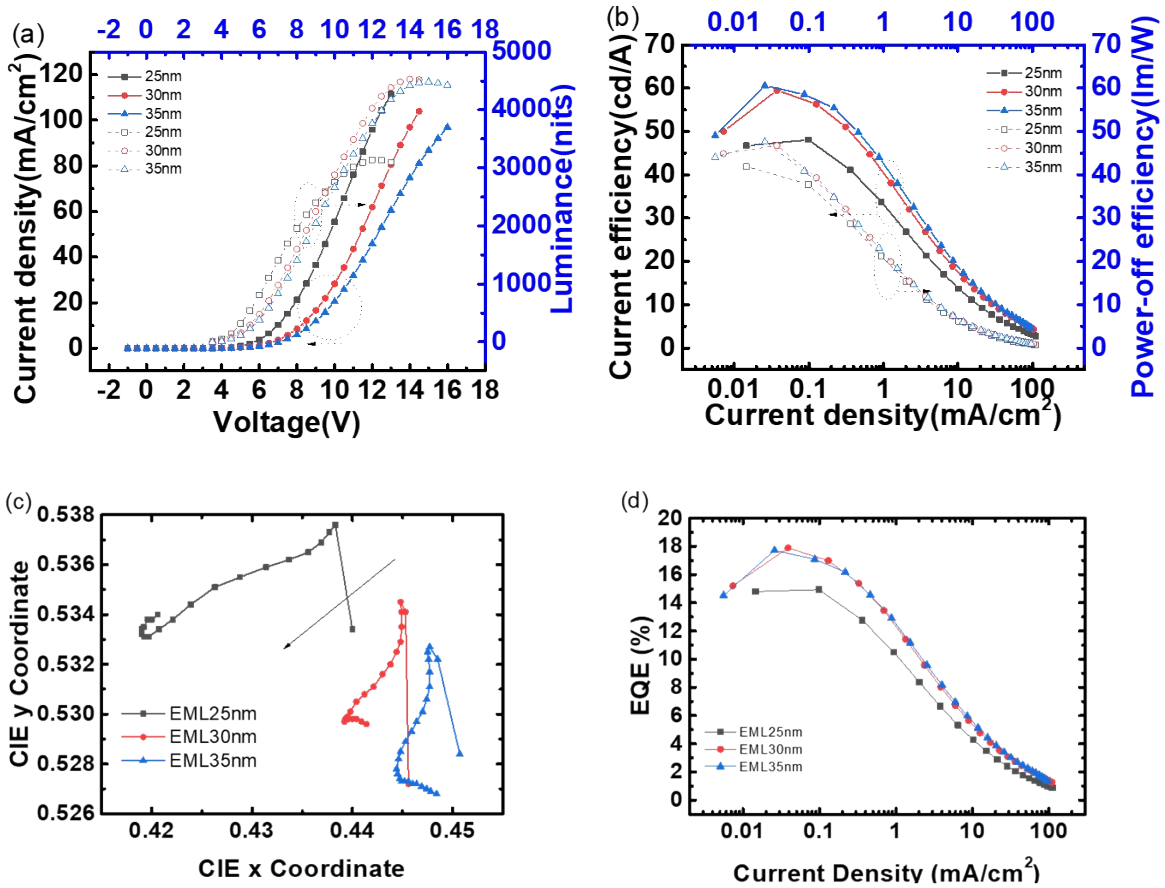

Fig. S27 EML thickness effects on the performance of the red TXO-TPA doped OLEDs (a) the J-L-V plots; (b) the current density-current efficiency-power efficiency curve; (c) CIE coordinate; (d) the current density- EQE curve.

Table S12 EML thickness effects on the performance of the red TXO-TPA doped OLEDs

Device entry	Driving Voltage (V)[a]	Max luminance (nits)	CE (cd/A)	PE (lm/W)	EQE (%)	LT50@ 1000nits (min)
EML25nm	5.03	3140	48.1[b], 18.5[d]	41.9[c], 9.3[d]	14.9[b], 5.8[d]	22[d]
EML30nm	5.79	4530	59.5[b], 26.5[d]	46.7[c], 11.9[d]	17.9[b], 7.9[d]	33[d]
EML35nm	6.09	4480	60.6[b], 29.5[d]	47.6[c], 12.7[d]	17.7[b], 8.7[d]	38[d]

[a]: J=1mA/cm^2. [b]: At max current efficiency. [c]: At max power off efficiency. [d]: At 1000nits.

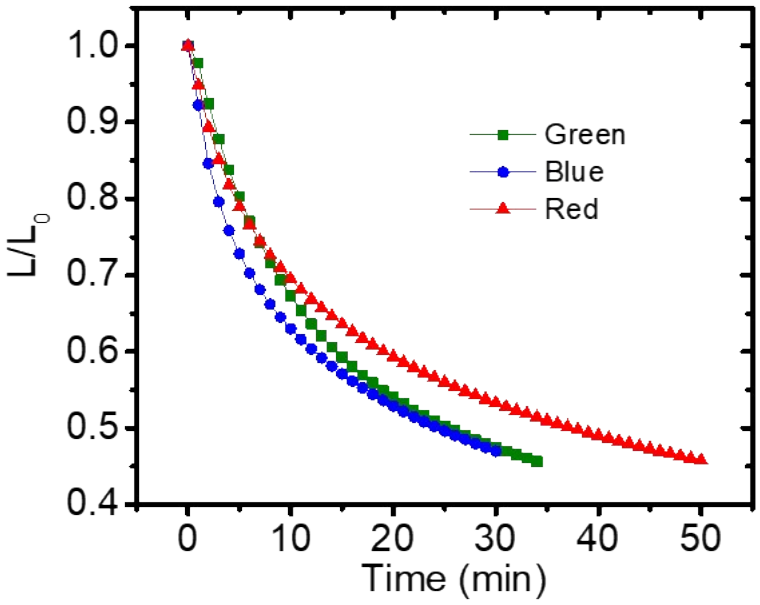

Fig. S28 The lifetime curve of the devices at 1000 nits: (i) the green line (-■-) represents the decay of the 4CzIPN doped green TADF-OLED. The device structure is ITO/TAPC (50 nm)/*m*CP (10 nm)/ **35Cbz4BzCN** doped **4CzIPN** (10 wt %) (30 nm)/DPPS (65 nm)/LiF (0.8 nm)/Al (120 nm); (ii) the blue line (-●-) represents the decay of **FIrpic** doped blue PhOLED device. The device structure is ITO/TAPC (50 nm)/*m*CP (10 nm)/ **35Cbz4BzCN** doped **FIrpic** (20 wt %) (30 nm)/DPPS (55 nm)/LiF (0.8 nm)/Al (120 nm); (iii) the red line represents the decay of the **TXO-TPA** doped red TADF device. The device structure is ITO/TAPC (50 nm)/*m*CP (10 nm)/ **35Cbz4BzCN** doped **TXO-TPA** (1 wt %) (30 nm)/DPPS (80 nm)/LiF (0.8 nm)/Al (120 nm). The sample devices had to expose to air during the change of the mask.

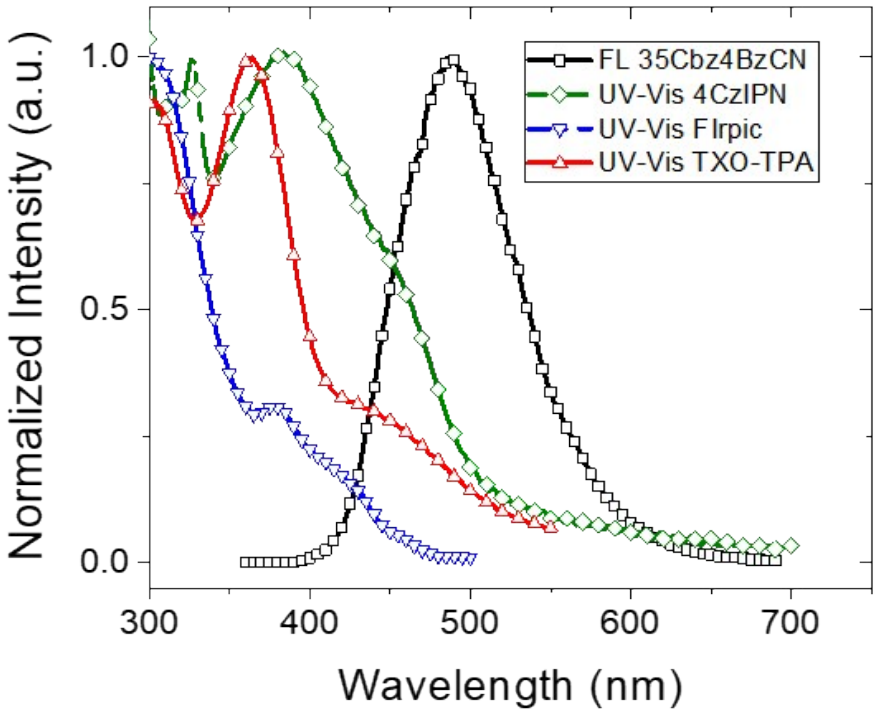

Fig. S29 Spectral overlap analysis of **35Cbz4BzCN** with the blue, green, and red emitters of FIrpic, 4CzIPN, and TXO-TPA. Since the emission spectrum of **35Cbz4BzCN's** has the λ_{max} longer than 490 nm (2.5 eV), energy transfer through FRET to FIrpic and perhaps to 4CzIPN may be less efficient.